NASA Contractor Report 4071

Eigenspace Techniques for Active Flutter Suppression

William L. Garrard, Bradley S. Liebst,
and Jerome A. Farm

GRANT NAG1-217
JUNE 1987

NASA

NASA Contractor Report 4071

Eigenspace Techniques for Active Flutter Suppression

William L. Garrard, Bradley S. Liebst,
and Jerome A. Farm
University of Minnesota
Minneapolis, Minnesota

Prepared for
Langley Research Center
under Grant NAG1-217

National Aeronautics
and Space Administration

**Scientific and Technical
Information Office**

1987

EIGENSPACE TECHNIQUES FOR ACTIVE FLUTTER SUPPRESSION

W. L. Garrard*, B. S. Liebst**, and Jerome A. Farm***
Department of Aerospace Engineering and Mechanics
University of Minnesota
Minneapolis, Minnesota 55455

SUMMARY

This report discusses the use of eigenspace techniques for the design of an active flutter suppression system for a hypothetical research drone. One leading edge and two trailing edge aerodynamic control surfaces and four sensors (accelerometers) are available for each wing. Full state control laws are designed by selecting feedback gains which place closed loop eigenvalues and shape closed loop eigenvectors so as to stabilize wing flutter and reduce gust loads at the wing root while yielding acceptable robustness and satisfying constraints on rms control surface activity. These controllers are realized by state estimators designed using an eigenvalue placement/eigenvector shaping technique which results in recovery of the full state loop transfer characteristics. The resulting feedback compensators are shown to perform almost as well as the full state designs. They also exhibit acceptable performance in situations in which the failure of an actuator is simulated.

---

*Professor
**Assistant Professor
***Graduate Research Assistant

Table Of Contents

List of Figures

List of Tables

List of Symbols

Vectors

c_i = i-th row of measurement matrix
u = control input
v_i = attainable closed loop eigenvector associated with λ_i eigenvalue
v_i^d = desired closed loop eigenvector associated with λ_i eigenvalue
w_i = vector used in calculation of gain matrix
x = system state
$\hat{x}$ = estimate of system state
y = measurement vector (accelerometer outputs)
Γ = disturbance input vector
ξ_s = vector of flexural generalized coordinates
ξ_c = control surface displacement vector
μ_i = the left zero-direction of the i-th finite transmission zero

Matrices

A_m = aerodynamic coefficient matrix
A = open loop dynamics matrix
B = control distribution matrix
C = measurement matrix
C_s = structural damping matrix
$G(s)$ = open loop transfer matrix, $C(sI-A)^{-1}B$
$F(s)$ = full state loop transfer matrix, $K(sI-A)^{-1}B$
$H(s)$ = compensator transfer matrix, $K(sI-A-BK+LC)^{-1}L$
$H(s)G(s)$ = loop transfer matrix
I = identity matrix
K = control gain matrix
L = estimator gain matrix
K_s = structural stiffness matrix
M_s = structural mass matrix
P_i = eigenvector weighting matrix associated with i-th eigenvector
$Q_c(s)$ = calculated unsteady aerodynamic influence coefficient matrix
$Q_A(s)$ = s-plane approximation of unsteady aerodynamic influence coefficient matrix

S = non-singular square matrix of order m
V = matrix whose columns are v_i
W = matrix whose columns are w_i

Scalars

$\overline{c}$ = local chord
c = reference chord, 14 inches
j = $\sqrt{-1}$
J_i = i-th performance index
L = reference length in Dryden gust model, 1700 ft
M = Mach number
m = number of controls
n = number of states
$\overline{q}$ = dynamic pressure
q = fictitious noise weighting
s = Laplace operator
V = forward velocity
z_i = i-th transmission zero
β_i = i-th aerodynamic lag frequency
η = zero mean white noise input to gust model, intensity (L/V) ξ_g^2
λ_i = i-th eigenvalue
ω = circular frequency
ξ_g = vertical wind gust velocity
ξ_g = rms vertical wind gust velocity
ϕ_i = influence coefficient associated with i-th flexure mode
$\underline{\sigma}(E)$ = minimum singular value of the matrix E
$\overline{\sigma}(E)$ = maximum singular value of the matrix E

Superscripts

d = desired
$*$ = complex transpose
T = transpose
-1 = inverse

Abbreviations

ARW	= Aero-Elastic Research Wing
DAST	= Drones for Aerodynamic and Structural Testing
LE	= leading edge
LQG	= linear quadratic Gaussian
LQR	= linear quadratic regulator
LTR	= loop transfer recovery
MIMO	= multi-input-multi-output
SISO	= single-input-single-output
TEI	= trailing edge inboard
TEO	= trailing edge outboard

SECTION 1

INTRODUCTION

This report describes a study of the use of eigenspace techniques for the design of an active flutter suppression/gust load alleviaton system for a mathematical model of a hypothetical flight test vehicle. Eigenspace techniques use feedback control to place closed loop eigenvalues and shape closed loop eigenvectors to achieve performance specifications. At the beginning of this study, aircraft applications of eigenspace techniques had been primarily in rigid body eigenvalue placement and modal decoupling to improve handling qualities [1,2,3,4]. Ostroff and Pines [5] used eigenvalue placement to design a flutter controller for a hypothetical aircraft, but did not attempt eigenvector shaping. More recently Alag, Burken, and Gilyard [6] applied eigenspace techniques to the design of of an output feedback system for suppression of non-symmetric flutter of an oblique-wing aircraft.

Active suppression of wing flutter can result in substantial weight savings and increases in performance compared with passive methods such as increased structural stiffness, mass balancing, and speed restrictions [7]; consequently, there has been considerable research on the development of techniques for the design of active flutter control systems. Much of this work has focused on the DAST (Drones for Aerodynamic and Structural Testing) ARW-1 and ARW-2 (Aeroelastic Research Wing) flight test vehicles. The DAST flight test vehicles are Firebee II Drones which have been modified by replacing the conventional wings with high aspect ratio, super-critical wings which are aerodynamically and structurally similar to those proposed for future air transports [8]. These wings are designed to flutter within the flight envelopes of the drones.

Several techniques have been used to design flutter control systems for the DAST vehicles. Abel, Perry and Murrow [9] compare two flutter control systems. One system design is based on classical single-input-single-output (SISO) feedback control techniques [10] and the other on the aerodynamic energy method of Nissim [11]. Newsom applies linear quadratic regulator (LQR) theory to the flutter suppression of the DAST wing [12] and Abel, Newsom, and Dunn describe an analytical and experimental comparison of the resulting controller with a controller designed using the aerodynamic energy approach [13]. Mahesh, Stone, Garrard and Dunn [14,15] use linear quadratic Gaussian (LQG) methodology coupled with the the Doyle-Stein procedure [16] for loop transfer recovery (LTR) to design a flutter controller for a full-sized wind tunnel model of the DAST wing. Mukhopadhyay, Newsom, and Abel present a method for designing a reduced-order LQR based controller for the DAST wing [17].

Newsom describes a practical flutter controller design based on LQR methodolgy for the DAST ARW-1 vehicle [18]. Schmidt and Chen [19] present a design based on classical SISO techniques for this aircraft and Adams and Tiffany [20] and Takahashi and Slater [21] discuss designs developed using LQG and LQR theory. Garrard and Liebst [22] compare full state eigenspace and LQR flutter controller designs for the DAST ARW-2 and Liebst, Garrard and Adams [23] use eigenspace techniques and frequency response matching to design a realizable feedback compensator for flutter suppression for this vehicle.

The flutter modes to be suppressed are symmetric; consequently, there are three sets of control surfaces on the actual DAST vehicle which could be considered for use in flutter suppression. These are (1) the elevator, (2) a set of flaps mounted inboard on each wing and (3) a set of ailerons mounted outboard on each wing. In the actual DAST vehicles the elevator is used for active control of the unstable short period longitudinal mode and for gust load alleviation, the inboard flaps are used for manuever load control and gust load alleviation, and the ailerons are used for flutter suppression. Since the ailerons operate symmetrically for suppression of symmetric flutter, flutter suppression systems for the actual DAST vehicles are SISO. All of the controller design techniques used in the studies listed above with the exception of classical SISO procedures are easily applied to the design of multi-input-multi-output (MIMO) control systems, and in fact the full power of these techniques is only apparent in MIMO systems. It is well known that in a controllable system with full state feedback and two or more control inputs, it is possible to place closed loop eigenvalues in any position and also to shape closed loop eigenvectors [24]. Dynamic response depends on both eigenvalue location and eigenvector shape, thus the ability to both explicitly place closed loop eigenvalues and shape closed loop eigenvectors is useful for the control system designer.

Since eigenstructure techniques are most useful when there are two or more control inputs, the authors of this report examined the use of the outboard ailerons in conjunction with both the flaps and the elevator. It was found that the flaps were ineffective for flutter control and attempts to include these surfaces seriously degraded stability margins compared with the use of the outboard ailerons alone [22]. The elevator is intended to control the longitudinal rigid body modes and inclusion of the elevator and rigid body modes along with the outboard ailerons and flexure mode simply resulted in a design which was essentially two SISO systems, one which controlled low frequency (rigid body) response with the elevator and the other which controlled high frequency (flexure mode response) with the outboard ailerons [23]. Since an adequate MIMO eigenspace controller could not be designed from mathematical models of the actual DAST vehicles, hypothetical control surfaces were added to the mathematical

model of the DAST ARW-2. Three possible surfaces were considered: the existing outboard aileron called the TEO (Trailing Edge Outboard) surface, an aileron just inboard of this surface called the TEI (Trailing Edge Inboard) surface, and an outboard leading edge (LE) surface. The locations of these surfaces and the four accelerometers available for measuring the motion of the wing are shown in Fig. 1. Designs which use all three surfaces and the LE and TEO surfaces only are studied.

Eigenstructure assignment can be achieved directly by least squares techniques [1-4,22,23] or asymptotically by LQR methods [25,26]. Both methods have advantages and disavantages. Full state MIMO LQR controllers have guaranteed good stability margins [27]; however, since a state estimator is almost always required in the feedback loop these margins may be lost in practice unless some type of LTR procedure is used to partially restore them. The direct approach does not result in guaranteed stability margins; however in practice margins are often good and Gilbert [28] has shown that sensitivity of eigenvalue location to parameter variations can be minimized if the closed loop eigenvectors are made as orthogonal as possible. The asymptotic LQR approach requires a controllable system while the direct approach does not and in fact can be used to shape eigenvectors associated with uncontrollable eigenvalues. The direct approach can be used to to design a gain matrix which acts on sensor outputs for direct output feedback. Also an eigenspace approach to the design of state estimators which exhibit LTR has recently been developed [29]. Finally the asymptotic LQR approach drives some closed loop eigenvalues to infinity. This may cause bandwidth problems. The direct approach can be used to maintain eigenvalues in their open loop position if the response associated with these eigenvalues is satisfactory and it is not desired to move them. For these reasons, the direct design approach is used in this study.

Eigenspace techniques are used to design full state control laws which stabilize the wing, reduce wing root gust loads, and result in good MIMO stability margins without exceeding limits on rms control surface deflections and rates. These full state controllers are then realized by use of dynamic state estimators. An eigenspace procedure which is very similar to the full state design procedure is used to design these state estimators so that they exhibit loop transfer properties which are very similar to the full state designs. The resulting compensators, which convert accelerometer outputs to actuator inputs, are shown to perform adequately even when the failure of a control surface is simulated.

The remainder of this report is divided into six major sections. In the first section, the performance requirements and mathematical models used in the study are described. Next the theory of eigenspace design is given for full state feedback and for estimators which exhibit LTR. The application of the theory to the design of full state flutter controllers

which also provide gust load alleviation is presented in the third section. This is followed by a description of the design of the state estimator used to realize the full state control laws. The final designs are given in the next section and the last section contains the conclusions.

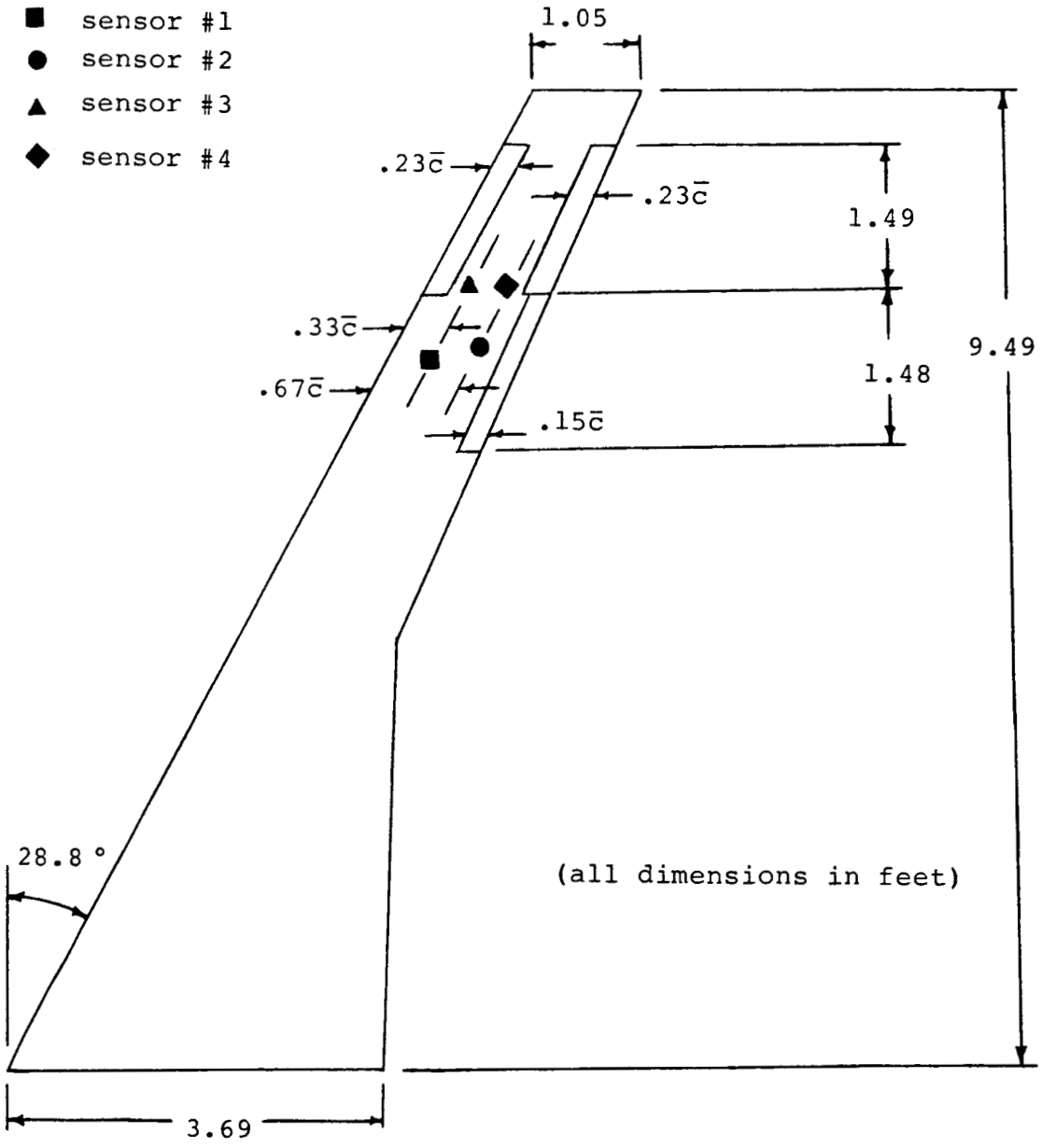

Figure 1: Planform of Wing

SECTION 2

PERFORMANCE REQUIREMENTS AND MATHEMATICAL MODELS

2.1 Aeroelastic Wing Model

The system to be modeled consists of the wing, a single leading and two trailing edge control surfaces, actuators, and a set of acclerometers used to sense the motion of the wing. The planform of the wing is shown in Fig. 1. The leading edge and two trailing edge control surfaces and the four accelerometer locations are indicated. The design flight condition is at a Mach number of 0.86 and an altitude of 15,000 ft (this corresponds to a velocity of 909 fps and a dynamic pressure of 4.29 psi). At this flight condition, the uncontrolled wing flutters and the flutter control system is required to stabilize the wing without exceeding rms control surface displacements of 15 deg and displacement rates of 740 deg/sec under a 12 fps rms vertical wind gust.

The aeroelastic model of the wing is given as

$$([M_s]s^2 + [C_s]s + [K_s])\,[\xi_s] + \bar{q}\,[Q_c(s)] \begin{Bmatrix} \xi_s \\ \xi_c \\ \xi_g \end{Bmatrix} = 0 \qquad (1)$$

In this form mass coupling between ξ_g and ξ_c has been neglected. $[Q_c(s)]$ is calculated as a function of reduced frequency by a doublet lattice procedure and is approximated by the matrix of transfer functions

$$[Q_A(s)] = [A_0]+[A_1][cs/2V]+[A_2][cs/2V]^2+\sum_{i=1}^{k}[A_{i+2}]s/(s+(2V/c)\beta_i) \qquad (2)$$

This type of model has been widely used to represent unsteady aerodynamic forces in the design of flutter control systems [8-23,30]. The usual procedure is to select the β_i's to span the reduced frequency range of interest and then choose the A_i's so as to give the best least squares fit to $[Q_c]$ over the range of reduced frequencies for which $[Q_c]$ is calculated. In a previous study, the authors selected the values of the β_i's in a different way [22]. An error matrix was defined as

$$E(j\omega) = [Q_c(j\omega) - Q_A(j\omega)]$$

The norm of this matrix is bounded above and below by its maximum and minimum singular values, i.e.,

$$\underline{\sigma}(E) \leq ||Ex||/||x|| \leq \overline{\sigma}(E)$$

The singular values of any matrix E are defined as the positive square roots of the eigenvalues of E*E. If the β_i's are chosen to minimize $\overline{\sigma}(E)$, the norm of the error matrix will be small. A single β_i with a value of 0.13 is used in this study, this is very close to the reduced flutter frequency of 0.15.

The model initially provided had two rigid body modes, heave and pitch, and eleven flexure modes. The flexure modes are shown in the appendix. Since the rigid body modes are at frequencies at least 50 times less than the lowest flexure mode, the rigid body modes were eliminated from the model. The resulting model has eleven degrees of freedom. The root locus of the eleven degree of freedom model for varying flight velocities at 15000 ft is shown in Fig. 2. It clearly indicates classical bending-torsion flutter with frequency coalescence of modes 1 and 3. The eigenvalues of the eleven degree system at the design flight condition of M = 0.86 and 15000 ft are given below.

Open Loop Eigenvalues - 11 Degree of Freedom Model

Mode Number	Real Part	Imaginary Part
1	6.037	±110.5
2	-0.349	±94.2
3	-44.460	±158.5
4	-1.359	±193.7
5	-2.091	±232.3
6	-14.720	±328.7
7	-22.530	±276.7
8	-6.700	±394.7
9	-13.040	±430.8
10	-16.790	±556.8
11	-6.970	±594.6

In order to reduce the order of the model, the root loci for various truncations of the model were obtained. Truncations were obtained by simply eliminating the rows and columns in the system dynamics matrix which correspond to the modes which were eliminated. To concisely present the results of this study, the eigenvalues of the flutter mode

(mode 1) at the design flight condition are shown for various truncations. The full 11 degree of freedom model is case 1.

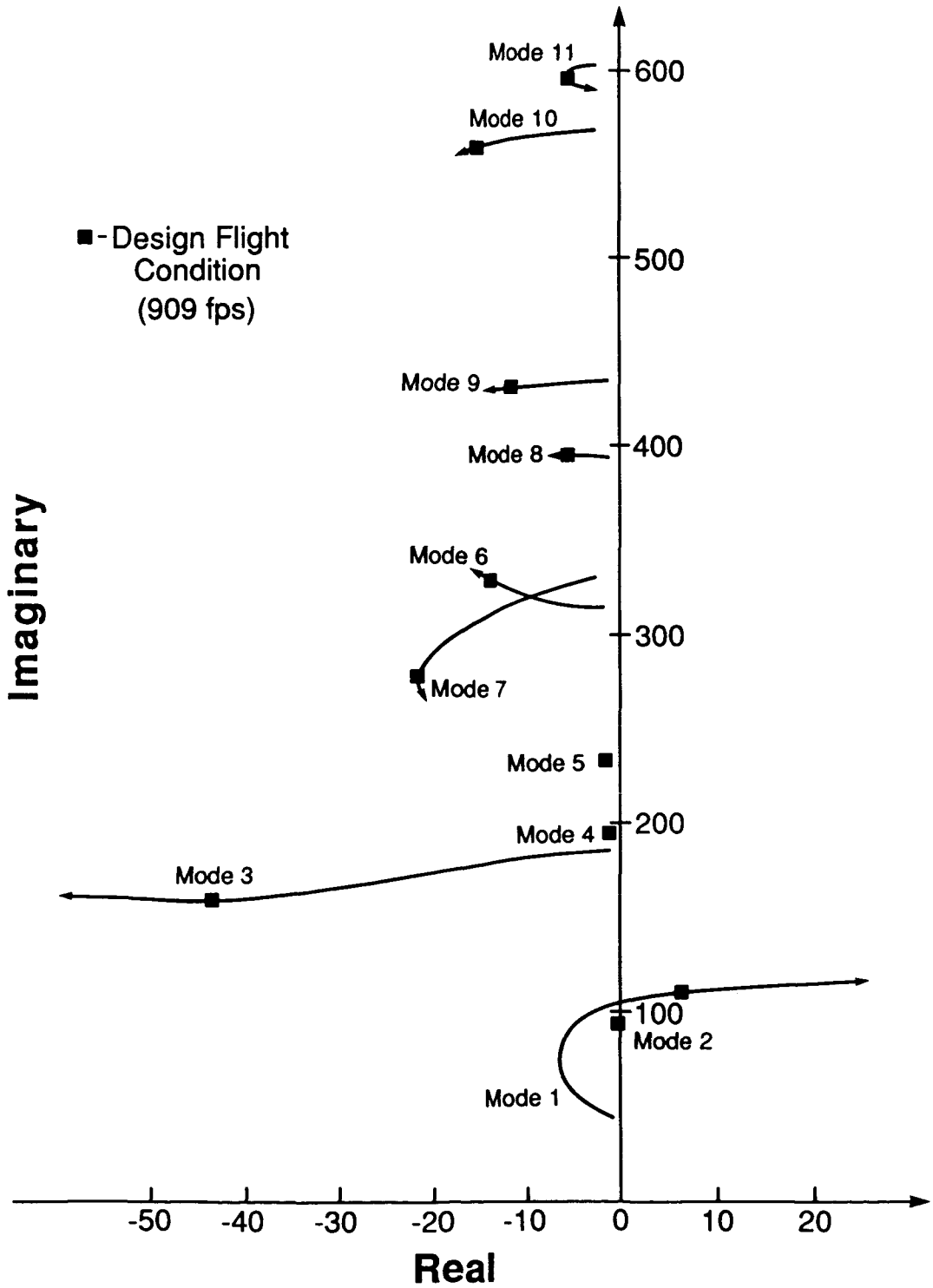

Figure 2: Locus of Open Loop Aeroelastic Roots with Velocity for Eleven Mode Model

Flutter Mode Root at Design Condition for Various Truncations

Case	Modes Retained	Model Degrees of Freedom	Mode 1 Root
1	1-11	11	6.037±j110.5
2	1-10	10	6.169±j110.7
3	1-5,7-11	10	5.453±j110.5
4	1-9	9	6.755±j110.9
5	1-4,7-11	9	4.014±j110.0
6	1-8	8	4.027±j111.5
7	1-7	7	3.158±j112.4
8	1-5,7,8	7	3.503±j111.6
9	1-5,7,9	7	3.580±j110.5
10	1-6	6	-8.135±j 80.7
11	1-5,7	6	0.053±j110.8
12	1-4,7,8	6	1.925±j111.0
13	1-4,7,9	6	2.097±j109.9
14	1-5	5	-8.234±j 80.5
15	1-4,7	5	-1.015±j110.0
16	1-4,8	5	-8.084±j81.0
17	1,2,4,6,7	5	-11.570±j96.1
18	1,3,4,5,7	5	1.190±j110.7
19	1,2,4,5,7	5	-11.430±j95.7
20	1,2,3,7,9	5	-0.040±j93.7
21	1,3,4,5,7,9	6	4.150±j110.5
22	1,3,4,7,9	5	2.700±j110.0
23	1-3,7	4	-9.521±j100.8

As the table shows, many of the lower order models do not exhibit flutter. Naturally modes 1 and 3 must be retained, however, which of the remaining modes to retain is not obvious. Examining the mode shapes, it can be seen that modes 2,5,6, and 8 are primarily fuselage and/or tail modes and therefore can be safely neglected. Examining cases 19 and 20, both modes 3 and 4 are necessary for flutter. Case 10 shows that mode 7 is also necessary for for flutter to occur. Cases 6 and 8 shows that mode 6 has little influence, Comparing cases 22 and 13, it can be seen that mode 2 can be neglected. Case 22 adequately represents the behavior of the wing with only 5 degrees of freedom. The root locus with velocity of this reduced order model as shown in Fig. 3 is very similar to original 11 degree of freedom model shown in Fig. 2; consequently, this model which contains modes 1,3,4,7,and 9 is used for the control designs. A structural damping factor of 0.005 is assumed for each mode and flutter occurs at a velocity of about 896 fps.

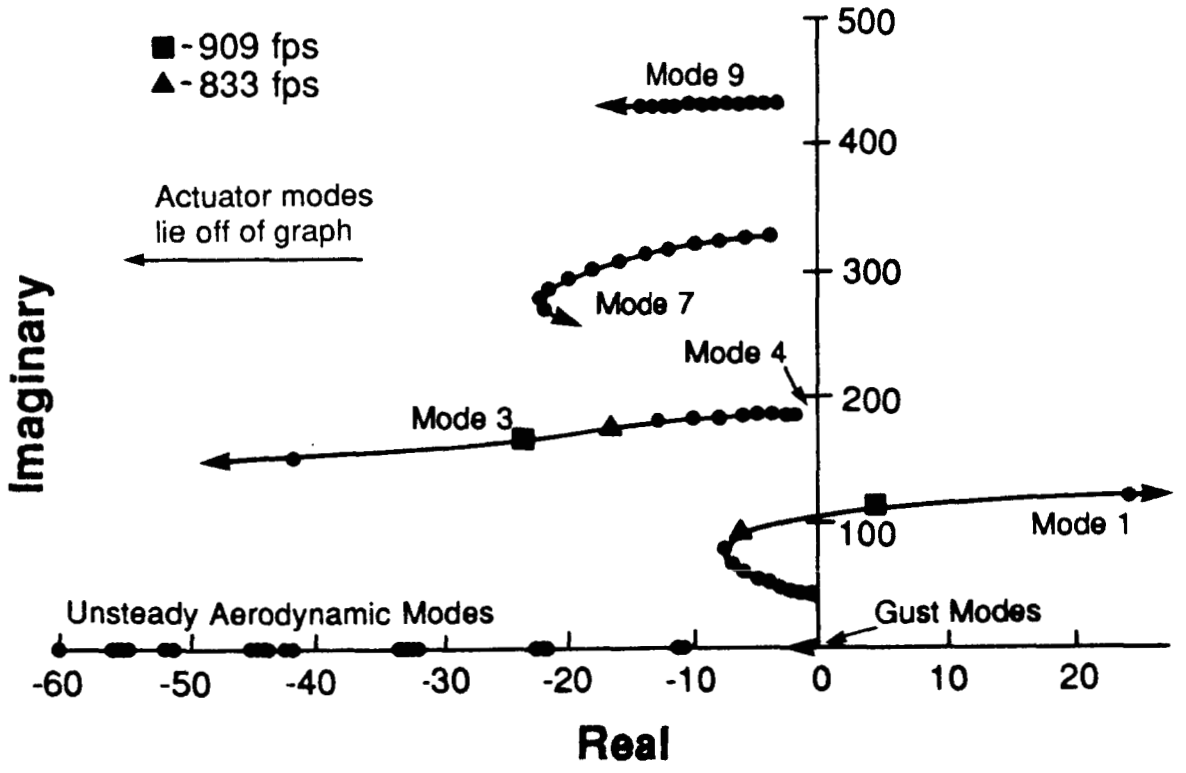

Figure 3: Locus of Open Loop Aeroelastic Roots with Velocity for Five Mode Model

2.2 Gust and Actuator Models

The control surface actuator transfer functions are the same for each surface and are given as

$$\xi_{ci}(s)/u_i(s) = 1.7744728x10^7/(s+180)(s^2+251s+(314)^2) \quad (3)$$

The vertical wind gust is modeled by a second-order Dryden model

$$\xi_g(s)/\eta(s) = [1+(\sqrt{3}\,L/V)s]/[1+(L/V)s]^2 \quad (4)$$

The rms gust velocity is 12 fps. For ease of recognition both the actuator poles and the gust poles were separated slightly in numeric calculations.

2.3 State Space Models

Equations (1-4) can be combined to give the mathematical model for the wing, control surfaces and actuators, and wind gust in vector matrix form as

$$\dot{x} = Ax + Bu + \Gamma\eta \quad (5)$$

The order of this model is 26. The state vector for the wing consists of five structural displacements, five corresponding rates, five unsteady aerodynamic states, nine control states (three for each surface), and two gust states. The motion of the wings can be sensed by up to four accelerometers mounted on the front and rear spars of each wing (see Fig. 1). The output of each accelerometer can be expressed as

$$\begin{aligned} y_i &= \sum \phi_i \dot{\xi}_{si} = f_i \dot{x} \\ &= f_i(Ax + Bu + \Gamma\eta) \\ &= f_i Ax + f_i Bu + f_i \Gamma\eta \end{aligned}$$

However, $f_i B = 0$ and $f_i \Gamma\eta$ is negligible, therefore

$$y_i = f_i Ax = c_i x \quad (6)$$

Thus the measurement vector is

$$y = Cx \quad (7)$$

Section 3

Theory of Eigenspace Design

A common method for the design of multivariable control systems is to use LQR theory to design full state controllers which achieve desired performance and to realize these controllers via Kalman filters which provide estimates of the system states [31]. For full state LQR controllers the minimum singular value of the return difference matrix is always greater than or equal to one. This guarantees gain margins of at least ±6 DB with no variations in phase, and phase margins of ±60 degrees with no variations in gain [27]. These stability margins are not necessarily retained if a Kalman filter is used in the feedback loop to estimate the system state [16]. However, stability margins of the full state controller can be recovered if the Kalman filter is designed using the LTR methods of Doyle and Stein [16]. This technique has been used in several studies of active flutter suppression systems [14,15,20].

In this report eigenspace techniques are used to design both full state control laws and estimators which result in compensators with loop transfer properties which approximate those of the full state controller. Eigenspace design techniques for full state feedback control laws select feedback gains which place closed loop eigenvalues in desired positions and which, if there is more than one control, shape closed loop eigenvectors. Some basic results for eigenspace design are summarized below. More detailed discussions can be found in Refs. 22-24 and 2.

3.1 Eigenspace Regulator Design

Consider a system described by Eq. 5 with a linear control law

$$u = Kx \tag{8}$$

where Dim(x)=n and Dim(u)=m if the system is controllable and B is full rank, the following results can be proven [2,24]:

1. The position of n closed loop eigenvalues can be arbitrarily assigned.
2. A total of m elements of each eigenvector can be arbitrarily selected.
3. The eigenvector associated with the eigenvalue λ_i, must lie in the subspace spanned by $(I\lambda_i\text{-}A)^{-1}B$.

If it is desired to move an eigenvalue, the design procedure consists of determining the gain matrix K such that for all desired closed loop eigenvalue and eigenvector pairs (λ_i, v_i),

$$(A+BK)v_i=\lambda_i v_i \tag{9}$$

This is equivalent to finding an m-dimensional vector w_i such that

$$(I\lambda_i-A)v_i=Bw_i \tag{10}$$

Once the w_i's have been found, the gain matrix is calculated as

$$K = W[V]^{-1} \tag{11}$$

Since the desired eigenvectors are in general not achievable, the w_i's are selected to minimize the weighted least squares difference between the elements of the desired and the attainable eigenvectors as given by the following performance index.

$$J_i = (v_i-v_i^d)^* P_i(v_i-v_i^d) \tag{12}$$

where P_i is a positive definite symmetric matrix whose elements can be chosen to weight the difference between certain elements of the desired and attainable eigenvectors more heavily than others. Adjoining Eq. 10 to J_i with the Lagrange multiplier υ_i, taking partial derivatives with respect to v_i and w_i, and setting these derivatives equal to zero, we get

$$N_i \begin{Bmatrix} v_i \\ w_i \\ \upsilon_i \end{Bmatrix} = \begin{Bmatrix} 0 \\ 0 \\ P_i v_i^d \end{Bmatrix}$$

where

$$N_i = \begin{bmatrix} (I\lambda_i-A) & -B & 0 \\ 0 & 0 & B^T \\ P_i & 0 & (I\lambda_i-A)^* \end{bmatrix}$$

If N_i is non-singular, the attainable v_i and w_i are then

$$\begin{Bmatrix} v_i \\ w_i \\ v_i \end{Bmatrix} = N_i^{-1} \begin{Bmatrix} 0 \\ 0 \\ P_i v_i^d \end{Bmatrix}$$

If an eigensolution is not to be altered, setting $w_i=0$ assures that the associated λ_i and v_i remain in their open loop configuration. In the case of a complex eigenvalue, a real gain matrix can be obtained from a simple transformation [24].

We will now show that whenever the system is controllable, N_i is in fact non-singular. First, consider the state equation transformed into diagonal form

$$\dot{x} = \Lambda x + Bu \qquad \Lambda = \begin{bmatrix} \lambda_1 & & & 0 \\ & \lambda_2 & & \\ & & \ddots & \\ 0 & & & \lambda_n \end{bmatrix}$$

Then

$$I\lambda_i - \Lambda = \begin{bmatrix} (\lambda_i-\lambda_1) & & & 0 \\ & (\lambda_i-\lambda_2) & & \\ & & \ddots & \\ 0 & & & (\lambda_i-\lambda_n) \end{bmatrix}$$

Now, assume the eigenvector weighting matrix P_i is diagonal, then N_i becomes

$$
N_i = \begin{array}{l} \text{rows} \\ \text{1 to n} \\ \\ \text{rows} \\ \text{n+1} \\ \text{to} \\ \text{n+m} \\ \\ \text{rows} \\ \text{n+m+1} \\ \text{to} \\ \text{2n+m} \end{array}
\begin{bmatrix}
(\lambda_i-\lambda_1) & \cdots & 0 & -b_{11} & \cdots & -b_{1m} & 0 & \cdots & 0 \\
\vdots & & \vdots & \vdots & & \vdots & \vdots & & \vdots \\
0 & \cdots & (\lambda_i-\lambda_n) & -b_{n1} & \cdots & -b_{nm} & 0 & \cdots & 0 \\
0 & \cdots & 0 & 0 & \cdots & 0 & b_{11} & \cdots & b_{n1} \\
\vdots & & \vdots & \vdots & & \vdots & \vdots & & \vdots \\
0 & \cdots & 0 & 0 & \cdots & 0 & b_{1m} & \cdots & b_{nm} \\
P_1 & \cdots & 0 & 0 & \cdots & 0 & (\lambda_i-\lambda_1)^* & \cdots & 0 \\
\vdots & & \vdots & \vdots & & \vdots & \vdots & & \vdots \\
0 & \cdots & P_n & 0 & \cdots & 0 & 0 & \cdots & (\lambda_i-\lambda_n)^*
\end{bmatrix}
$$

To prove that N_i is nonsingular, we need only prove N_i has rank 2n+m or that all possible sums of multiples of rows will not result in a zero row. If we have a controllable system the first n+m rows have rank n+m for all values of the desired eigenvalue λ_i. Since P_i is positive definite, the last n rows have rank n. Last, if P_i is positive definite the last n rows could never cancel the first n+m rows and vice versa.

If the system is uncontrollable, transforming it to the controllability canonical form would easily show that the first n+m rows of N_i would not have rank n+m when λ_i was one of the uncontrollable eigenvalues. Solutions for eigenvector shaping of an uncontrollable eigenvalue λ_g (the gust eigenvalue in the present problem) can still be obtained, however. This problem can be solved by partitioning the eigenvector v_g associated with the eigenvalue λ_g as follows

$$
\left[\begin{array}{c|c} (\lambda_g I - A^I) & Q \\ \hline 0 & R \end{array}\right]
\left\{\begin{array}{c} v_g{}^I \\ \hline v_g{}^{II} \end{array}\right\} =
\left\{\begin{array}{c} B^I \\ \hline 0 \end{array}\right\} w_g
$$

where $v_g{}^{II}$ contains only uncontrollable states. The equation

$$
R v_g{}^{II} = 0
$$

is automatically satisfied if v_g^{II} is selected to be equal to the open loop portion of v_g which contains the uncontrollable states. Since λ_g is not an eigenvalue of A^I, $(\lambda_g I - A^I)$ is non-singular and by performing the indicated calculations, w_g and v_g^I can be determined in much the same way as for the controllable eigenvalues

$$\begin{Bmatrix} v_g^I \\ w_g \\ v_g \end{Bmatrix} = N_g^{-1} \begin{Bmatrix} -Q\, v_g^{II} \\ 0 \\ P_g\, v_g^{Id} \end{Bmatrix}$$

where

$$N_g = \begin{bmatrix} (\lambda_g^I - A^I) & -B^I & 0 \\ 0 & 0 & B^{IT} \\ P_g & 0 & (\lambda_g^I - A^I)^* \end{bmatrix}$$

Once all w_i's and v_i's have been calculated the regulator gain matrix is determined from Eq. 11.

3.2 Eigenspace Estimator Design

Once the full state regulator gains, K, have been determined the problem of reconstructing a state estimate, $\hat{x}$, from measurements, y, must be addressed. A common estimation/control scheme is as follows

$$u = K\hat{x}$$

Where

$$\dot{\hat{x}} = A\hat{x} + Bu + L(y - C\hat{x})$$

By appropriate choice of K we have demonstrated how to achieve the desired closed loop eigenstructure of the plant. However, that was under the assumption of full state feedback. The task now is to choose estimator gains, L, such that A - LC is stable and the performance (as measured by various methods, e.g. transfer functions, rms response, stability robustness, etc.) of the regulator/estimator closely resembles that of full state feedback. In the Kalman filter L is chosen to produce an estimate that has minimal mean square reconstruction error $e = x - \hat{x}$ to uncorrelated additive white plant and measurement noises. But as pointed out by various authors

[16] the Kalman filter may not be robust even when the full state regulator is. For MIMO systems the stability robustness is typically measured by the minimum singular value of the return difference matrix occuring in a bounded frequency range. A value near one for this minimum singular value indicates good stability robustness [31]. In the full state feedback case the return difference matrix is

$$I - F(s)$$

Where

$$F(s) = K (sI - A)^{-1} B$$

and in the combined regulator/estimator case it is

$$I - H(s)\, G(s)$$

Where

$$H(s) = K (sI - A - BK + LC)^{-1} L$$

$$G(s) = C (sI - A)^{-1} B$$

In the SISO case it is clear that if one wishes to recover F(s) then L should be chosen such that

$$H(s) \approx F(s) / G(s)$$

inverting the plant by sending the poles of H(s) to the zeros of G(s). Care must be taken to assure that the eigenvalues of the estimator, A - LC, are stable. In the MIMO case it is less clear how one would invert the plant and recover F(s).

A technique for designing L in the MIMO case to recover F(s) was proposed by Doyle and Stein [16]. They showed that LTR of full state regulators can be achieved with a Kalman estimator by adding a fictitious noise q^2BB^T directly to the input of the plant during the estimator design. For q=0 the ordinary Kalman estimator results. As q is increased the LTR improves resulting in the recovery of full state stability robustness. A key result from Ref. 16 is that as $q \rightarrow \infty$ the estimator gains $L \rightarrow qBS \rightarrow \infty$, and the estimator poles asymptotically approach the finite transmission zeros of G(s) (ie plant inversion) and infinity in a Butterworth pattern. Several investigators (the present authors included) seized upon this fact to attempt to achieve LTR with eigenspace assignment algorithms as opposed to Kalman filter algorithms by directly placing the estimator poles at (or

near) the plant transmission zeros.

In a multivariable system, the zeros of the individual transfer functions no longer correspond to the classical notion of zeros. In a SISO system as the elements of the output feedback matrix are allowed to approach infinity the closed loop poles of the estimator approach the locations of the finite zeros (or infinity if there is an excess) of the plant. As demonstrated by the Doyle-Stein LTR procedure the equivalent occurs in MIMO systems. The closed loop estimator poles approach the finite transmission zeros of G(s) which can be determined from

$$\det \begin{bmatrix} z_i I - A & B \\ -C & 0 \end{bmatrix} = 0 \qquad (13)$$

Unfortunately, it is not quite as simple as just sending the estimator poles to the transmission zeros. A recent paper by Kazerooni and Houpt [29] explains how LTR is achieved with eigenspace placement.

The key lemma to successful LTR with eigenspace placement is the following result which is proved in Ref. 16. If L is chosen such that

$$\frac{L(q)}{q} \rightarrow BS \qquad \text{as} \qquad q \rightarrow \infty \qquad (14)$$

then H(s) approaches pointwise (ie, nonuniformly)

$$K(sI - A)^{-1}B \left[C(sI - A)^{-1} B\right]^{-1}$$

and therefore

$$H(s)\, G(s) \rightarrow F(s) \qquad (15)$$

Thus, by picking

$$L = qBS \qquad (16)$$

Eq. 14 will be satisfied and the LTR of Eq. 15 will be achieved as $q \rightarrow \infty$. Ref. 29 shows that, for a minimum phase plant, as $q \rightarrow \infty$ the consequences of choosing L as in Eq. 16 are:

1. The $j \leq n\text{-}m$ finite closed loop eigenvalues, λ_j, of A-LC and A + BK -LC approach the finite transmission zeros, z_j, of the plant.

2. The remaining n-j closed loop eigenvalues approach infinity at any angle.

3. The left closed loop eigenvector v_i of A-LC associated with the finite closed loop estimator eigenvalue, λ_i, approaches the left zero-direction, μ_i, of the transmission zero, z_i, which satisfies

$$[\ \mu_i^T \quad \zeta_i^T\ ] \begin{bmatrix} z_i I - A & B \\ -C & 0 \end{bmatrix} = 0 \qquad (17)$$

4. H(s) G(s) → F(s) pointwise.

The finite asymptotic eigenstructures resulting from both Eq. 14 and Eq. 16 are the same, but the asymptotic infinite eigenstructures are generally different. If S is selected arbitrarily, the form of L given by Eq. 16 may not result in a stable estimator. Since both forms guarantee the pointwise approach of H(s)G(s) to F(s) we would expect any estimator with the finite asymptotic structure of 1. thru 3. to achieve LTR. Therefore, for a minimum phase system, an estimator which combines any stable infinite eigenstructure with the finite eigenstructure of 1. thru 3. would result in LTR.

The procedure for the design of estimators which achieve LTR with the eigenspace placement algorithms previously described is as follows:

1. Determine the finite transmission zeros, z_i, and associated left zero-directions, μ_i, from Eq. 17.

2. Drive j finite eigenvalues of A-LC to (or near) the finite transmission zeros, z_i. The associated desired (and in this case, attainable) left eigenvectors should be chosen as μ_i.

3. Place the remaining n-j eigenvalues of A-LC at locations far into the left-half plane. The desired left eigenvectors for these modes are chosen arbitrarily and have little effect on the LTR.

4. As with the Doyle-Stein procedure, improved LTR is obtained as the finite eigenvalues are moved closer to the transmission zeros and as the infinite eigenvalues are moved further left. Therefore, several iterations may be required before sufficient recovery is achieved.

Difficulties in using this LTR procedure will arise if the plant has right-half plane transmission zeros (ie, nonminimum phase). Placing the estimator poles at these right-half plane zeros would result in an unstable system, admittedly with good LTR, but nonetheless unstable. In the case of a nonminimum phase plant, the Doyle-Stein procedure selects the stable Riccati solution for the estimator which drives the poles to the mirror image of any unstable transmission zeros. Thus, a stable estimator is obtained but LTR is not guaranteed. If there are no right-half plane transmission zeros in the frequency range over which LTR is important, then placement of estimator poles at the mirror image of right-half plane transmission zeros typically achieves reasonable LTR.

Section 4

Full State Feedback Design

4.1 Eigenstructure Assignment

In the discussion which follows, unless otherwise stated, all results are for a control system using all three control surfaces. In flutter suppression/gust load alleviation designs in this report all of the stable open loop eigenvalues are used as desired closed loop eigenvalues. However, at the design velocity the aircraft's wing is unstable in the first bending mode, yielding a pair of unstable eigenvalues at +2.698±j109.9. Two closed loop positions are considered for these eigenvalues. The first position is obtained simply by "flipping" the unstable eigenvalues into the left-half plane to -2.698±j109.9 as minimum energy LQR theory would place them [32]. The second position, -8.1±j109.9, is obtained by moving the eigenvalues twice as far to the left as they move when they are simply flipped.

Figs. 4 and 5 show how rms bending moment, torque and singular value vary with elastic mode weighting. It can be seen that the -8.1±j109.9 placement yields higher minimum singular values and hence a more robust system than the -2.698±j109.9 placement. (In general, references to minimum singular value should be taken to mean the smallest minimum singular value of the return difference matrix which occurs over a bounded frequency range at some fixed flight velocity.) In addition, comparing the first column of Table 1 with that of Table 2 reveals that this placement doesn't cost significantly more in terms of control effort (when using the decoupled eigenvectors described below), while the triangular points in Fig. 4 show that bending moment is unchanged. Comparing the triangular points in Fig. 5 reveals that torque is actually reduced by using this placement.

Using -8.1±j109.9 for the desired mode 1 eigenvalues, and the open loop eigenvalues for the remaining desired closed loop eigenvalues, the desired eigenvectors are then selected. Using the open loop eigenvectors as is done for the triangular points in Figs. 4 and 5 provides a simple means of selection, but not the most effective. By decoupling the first bending mode from the other modes a 25% reduction in bending moment is obtained. With only three controls to shape the eigenvectors, the actual decoupling which results is of course only partial. The desired eigenvectors to achieve this decoupling are obtained by performing the following modifications upon the open loop eigenvectors. In the desired first bending mode eigenvector, the elements corresponding to structural modes 3, 4, 7 and 9, their corresponding unsteady aerodynamic elements, and the control mode elements are set to zero to minimize the energy in

	Weightings				
	Elastic Modes				
	1	10	100	1000	10000
	RMS Responses				
	Control Deflections (deg)				
TE Outboard	3.077	7.359	14.69	12.6	11.21
TE Inboard	9.425	3.836	0.8752	1.91	3.956
LE	3.873	11.83	20.28*	24.22*	23.74*
	Control Rates (deg/sec)				
TE Outboard	47.36	95.43	168.7	142.4	124.1
TE Inboard	117.2	51.95	9.2	25.7	50.42
LE	59.63	137.5	229.6	277.2	275.4

* Saturated

Table 1: Effects of Increasing Elastic Mode Weightings on RMS Control Surface Activity (Mode 1 Pole: -2.698±j109.9)

	Weightings				
	Elastic Modes				
	1	10	100	1000	10000
	RMS Responses				
	Control Deflections (deg)				
TE Outboard	3.074	7.368	14.7	12.6	11.21
TE Inboard	9.438	3.845	0.878	1.912	3.958
LE	3.890	11.84	20.28*	24.22*	23.74*
	Control Rates (deg/sec)				
TE Outboard	49.69	97.44	167.9	141.4	123.2
TE Inboard	123.7	56.21	10.94	25.62	50.3
LE	66.18	139.7	229.2	276.5	275.0

* Saturated

Table 2: Effects of Increasing Elastic Mode Weightings on RMS Control Surface Activity (Mode 1 Pole: -8.1±j109.9)

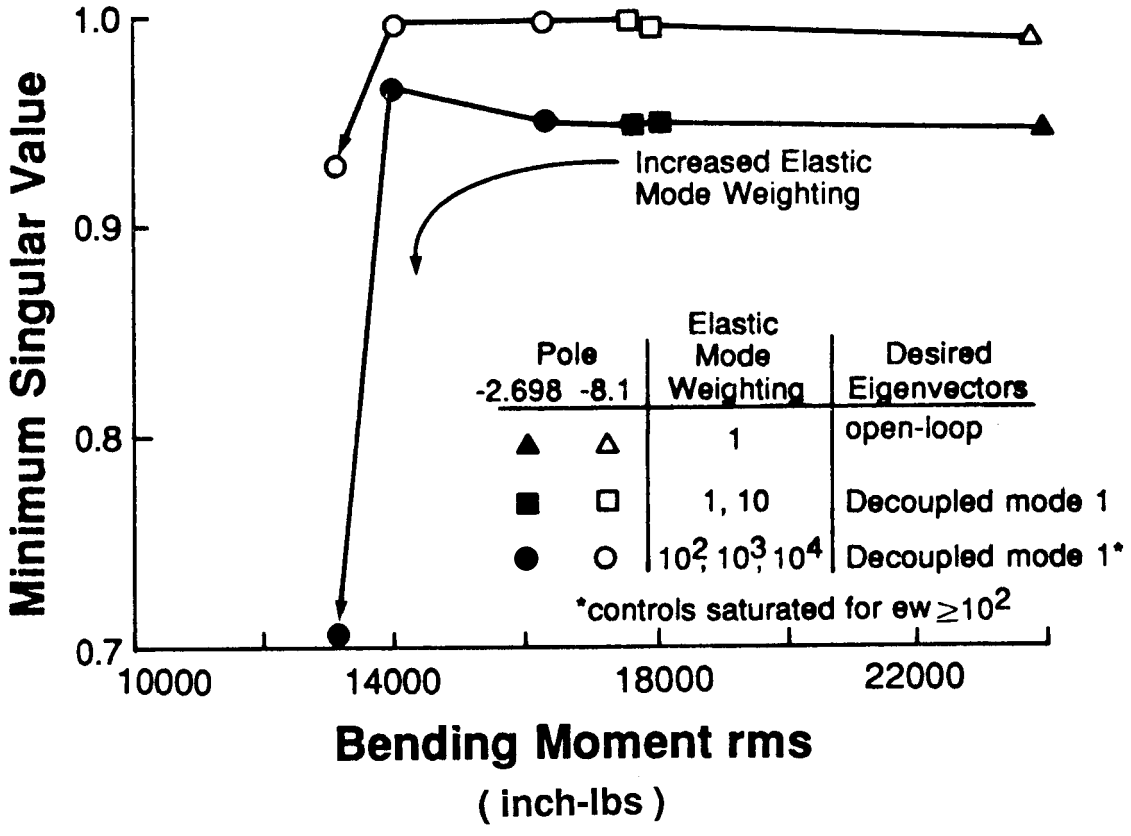

Figure 4: Effect of Elastic Mode Weighting and Eigenvalue Placement on Bending Moment and Minimum Singular Value

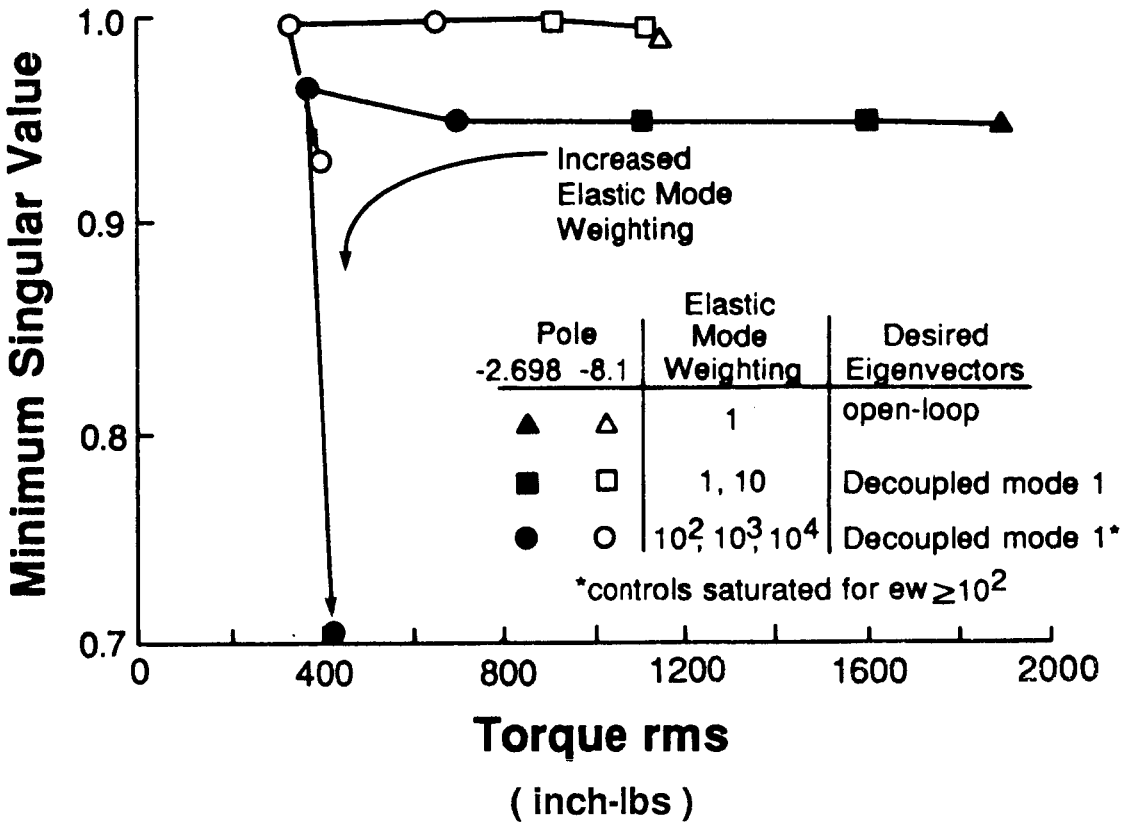

Figure 5: Effect of Elastic Mode Weighting and Eigenvalue Placement on Torque and Minimum Singular Value

the first bending mode and to reduce the control effort. In all of the other eigenvectors, the elements corresponding to the first bending mode's displacement and rate and to the first unsteady aerodynamic mode are set to zero in order that the other modes do not excite the first bending mode. The reduction in bending moment is found to arise largely from the zeroing of the first bending mode elements in the desired gust mode eigenvectors. A lesser reduction is achieved in torque since the first bending mode has a small torque component.

4.2 Eigenvector Weighting

By altering the P_i in Eq. 12 to increase the weightings on the elastic mode elements of the eigenvectors when finding v_i, the elastic mode elements are made to approach the desired zero values more closely. This improves the bending mode decoupling described above, consequently reducing bending moment and torque loads. The arrows in Figs. 4 and 5 indicate the downward trend in structural loads as the elastic mode weightings increase. Elastic mode weightings of 100 or greater lead to saturation of the LE surface, as shown in Tables 1 and 2. The minimum singular values are nearly constant as elastic mode weightings increase to 10000, at which point the minimum singular values drop off sharply. This suggests that the structural loads can be further reduced with no loss in robustness if the LE control could be kept from saturating. Note that the drop in minimum singular value is less severe for the $-8.1 \pm j109.9$ eigenvalue position, falling only to 0.929 compared to 0.706 for the other position.

Since only the LE control is saturating and the workload is not evenly distributed between the controls, the control weightings are altered to force the system to distribute the workload more evenly between the control surfaces. By increasing the weightings for eigenvector components corresponding to a particular control surface, those components are made to agree more closely with the desired value of zero. As a result, that surface works less, while the others will work more. Tables 3, 4, and 5 show various control weightings and the corresponding results for elastic mode weightings of 100, 1000, and 10000, respectively. The results are summarized in Fig. 6.

By evenly distributing the workload, LE control saturation is avoided and it is possible to increase the elastic mode weighting to 10000. This allows a 50% reduction in bending moment compared to the 25% reduction possible without distributing the workload. The drop in minimum singular value to 0.929 at this elastic mode weighting is judged to be acceptable. Using the results of Ref. 33, this corresponds to a +23,-5.7 DB MIMO gain margin (with no change in phase) and a ±55 degree MIMO phase margin (with

Velocity (fps)	909	909	909	909	833	833
Weightings						
Elastic Modes						
	100	100	100	100	-	100
Control Surfaces						
TEO (x,v,a)**	1,1,1	5,5,5	5,1,1	7,1,1	-	7,1,1
TEI (x,v,a)	1,1,1	1,1,1	1,1,1	1,1,1	-	1,1,1
LE (x,v,a)	1,1,1	4,4,4	4,1,1	7,1,1	-	7,1,1
RMS Responses						
Control Deflections (deg)						
TE Outboard	14.7	10.9	12.61	11.73	0.	11.23
TE Inboard	0.878	9.742	6.612	9.467	0.	10.87
LE	20.28*	9.599	12.22	8.645	0.	8.136
Control Rates (deg/sec)						
TE Outboard	167.9	125.0	143.6	133.9	0.	119.3
TE Inboard	10.94	128.9	87.53	122.1	0.	128.1
LE	229.2	109.5	137.5	98.35	0.	85.47
Bending Moment (inch-lbs)						
	16350	15820	16350	16350	22980	13260
Shear (lbs)						
	464.8	447.4	460.7	459.3	412.1	393.2
Torque (inch-lbs)						
	650.1	1926	1611	2049	817.5	1747
Minimum Singular Value						
	0.997	0.673	0.997	0.997	-	0.970

* Saturated

** x = displacement, v = rate, a = acceleration

Table 3: Effects of Distributing Control Surface Workload on RMS Control Surface Activity (Elastic Mode Weighting = 100)

Velocity (fps)	909	909	909	909
Weightings				
Elastic Modes				
	1000	1000	1000	1000
Control Surfaces				
TEO (x,v,a)**	1,1,1	5,5,5	5,1,1	5,1,1
TEI (x,v,a)	1,1,1	1,1,1	1,1,1	1,1,1
LE (x,v,a)	1,1,1	7,7,7	7,1,1	10,1,1
RMS Responses				
Control Deflections (deg)				
TE Outboard	12.6	10.95	11.67	11.69
TE Inboard	1.912	11.98	9.02	10.57
LE	24.22*	11.12	14.56	12.09
Control Rates (deg/sec)				
TE Outboard	141.4	124.5	131.8	132.3
TE Inboard	25.62	148.8	112.7	131.1
LE	276.5	127.7	164.5	136.6
Bending Moment (inch-lbs)				
	14010	14210	14310	1452
Shear (lbs)				
	425.4	434.3	435.3	440.9
Torque (inch-lbs)				
	331.2	2039	1579	1908
Minimum Singular Value				
	0.995	0.631	0.995	0.995

* Saturated

** x = displacement, v = rate, a = acceleration

Table 4: Effects of Distributing Control Surface Workload on RMS Control Surface Activity (Elastic Mode Weighting = 1000)

Velocity (fps)	909	909	909	833	833
Weightings					
Elastic Modes					
	10000	10000	10000	-	10000
Control Surfaces					
TEO (x,v,a)**	1,1,1	7,1,1	1,1,1	-	1,1,1
TEI (x,v,a)	1,1,1	1,1,1	1,1,1	-	1,1,1
LE (x,v,a)	1,1,1	35,1,1	35,1,1	-	35,1,1
RMS Responses					
Control Deflections (deg)					
TE Outboard	11.21	10.3	10.49	0.	10.07
TE Inboard	3.958	10.94	10.68	0.	11.4
LE	23.74*	14.56	14.62	0.	14.33
Control Rates (deg/sec)					
TE Outboard	123.2	114.6	116.7	0.	105.3
TE Inboard	50.3	134.0	131.1	0.	130.5
LE	275.0	168.3	168.9	0.	155.8
Bending Moment (inch-lbs)					
	13160	13390	13490	22980	11240
Shear (lbs)					
	409.0	417.8	419.9	412.1	363.5
Torque (inch-lbs)					
	399.3	1620	1611	817.5	1336
Minimum Singular Value					
	0.929	0.929	0.929	-	0.904

* Saturated

** x = displacement, v = rate, a = acceleration

Table 5: Effects of Distributing Control Surface Workload on RMS Control Surface Activity (Elastic Mode Weighting = 10000)

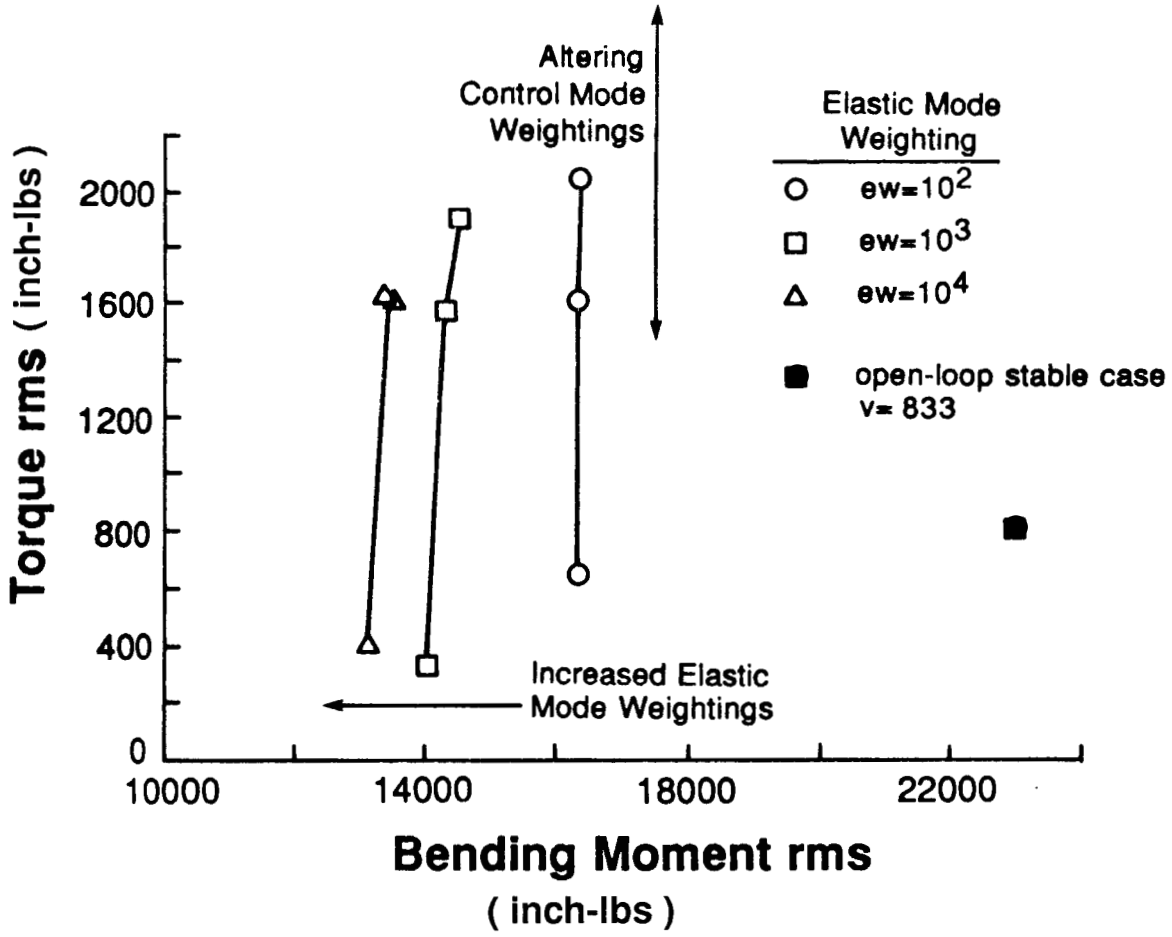

Figure 6: Effect of Elastic Mode Weighting and Control Mode Weighting on Torque and Bending Moment

no change in gain).

In Fig. 6 it can be seen that the bending moment depends largely upon the elastic mode weightings and is relatively insensitive to the control mode weightings. Since all of the control surfaces are near the tip of the wing, they have nearly the same moment arm and roughly equal effectiveness in reducing bending moment. It can also be seen that torque depends greatly on control mode weightings. By evenly distributing the actuator workload, a torque imbalance is created between the two trailing edge surfaces and the single leading edge surface. Thus, even distribution of the workload between the three surfaces allows elastic mode weightings to be increased to reduce bending moment, but at the expense of increased torque.

An interesting effect may be seen in Tables 3 and 4. Compare, for example, columns two and three in Table 3. In column two, weightings are increased on control surface deflections, rates, and accelerations, resulting in a seriously degraded minimum singular value. For column three, weightings are increased only on control deflections and the minimum singular value is unchanged. Since the designs represented in columns two and three are equally effective in distributing the control efforts, only the weightings for control deflection are modified in subsequent designs in order to preserve robustness.

In Tables 1 and 2 it can be seen that the TE inboard surface does not work very hard for higher elastic mode weightings. Since the TE inboard surface is actually smaller and has a smaller moment arm than the the TE outboard surface, it is not quite as effective as the other surfaces in reducing bending moment, and the controller does not "use" it very much.

Since the control effort of the TE inboard surface is low, and since making it work more causes a torque imbalance, a two-control system without the TE inboard surface is examined as well. Removing this surface from the system reduces the order of the system to 23. This system exhibits higher bending moment and lower torque than the three-control case due to the lack of the TE inboard surface. The two-control case has higher minimum singular values as well. This illustrates the conservative nature of utilizing the minimum singular value of the return difference matrix as a stability robustness measure.

4.3 Final Full State Designs

Based on the performances of the different designs and trade-offs between gust load alleviation and stability robustness, two eigenvector weighting schemes are chosen as candidates for the full state design, one each for the three- and two-control cases. The first is a three-control system using elastic mode weightings of 10000. The main features of this design are that it has the lowest bending moment of any of the designs,

with torque and minimum singular value which compare favorably to other weighting schemes. The second scheme, for the two control case, uses elastic mode weightings of 100. Its main features are high minimum singular value and low torque.

These two full state designs have control deflections which are near saturation. To avoid saturation problems due to possible increases in control deflections when the state estimator is added to the system, the control mode weightings are increased to reduce the control deflections. This later proves to be unnecessary.

This completes the full state designs, which are shown in Table 6. At the design velocity both the two- and three-control systems are stable and robust. Also shown are the performances of the two closed loop systems and the open loop system at a flight velocity of 833 fps at which the open loop system is stable. Again both closed loop systems are stable and robust, and also provide gust load alleviation by reducing bending moment, though at the expense of an increase in torque.

The effects of a single, undetected control surface failure on the full state feedback systems are examined by zeroing the column corresponding to the failed control in the control gain matrix K. As shown in Table 7, the loss of a control surface greatly reduces the minimum singular value. However, even though robustness is lost, the system is still nominally stable at the design velocity.

The loss of a control surface also has a marked effect on torque, such as in the two-control case where the failure of either surface nearly doubles the torque. In the three-control case, failure of one of the trailing edge surfaces actually reduces the torque since the remaining trailing edge surface and the LE surface then balance each other. Conversely, failure of the leading edge surface leaves the two trailing edge surfaces unbalanced and the torque becomes quite high.

	3-control	2-control	Open Loop	3-control	2-control
Velocity (fps)	909	909	833	833	833
			Weightings		
			Elastic Modes		
	10000	100	-	10000	100
			Control Surfaces		
TEO (x,v,a)*	60,1,1	90,1,1	-	60,1,1	90,1,1
TEI (x,v,a)	110,1,1	1,1,1	-	110,1,1	1,1,1
LE (x,v,a)	120,1,1	60,1,1	-	120,1,1	60,1,1
			RMS Responses		
			Control Deflections (deg)		
TE Outboard	11.97	10.09	0.	11.77	9.92
TE Inboard	10.49	-	0.	10.82	-
LE	11.91	8.878	0.	11.92	8.71
			Control Rates (deg/sec)		
TE Outboard	135.0	129.6	0.	125.1	113.4
TE Inboard	126.3	-	0.	121.1	-
LE	139.7	114.7	0.	130.4	101.0
			Bending Moment (inch-lbs)		
	14600	20550	22980	12000	20550
			Shear (lbs)		
	440.0	474.8	412.1	382.8	474.8
			Torque (inch-lbs)		
	1945	1048	817.5	1574	1048
			Minimum Singular Value		
	0.929	0.996	-	0.904	0.972

* x = dispacement, v = rate , a = acceleration

Table 6: Final Full State Feedback Designs

	3-control			2-control	
			Failed Control		
	TEO	TEI	LE	TEO	TEI
			RMS Responses		
			Control Deflections (deg)		
TE Outboard	-	13.12	12.73	-	10.31
TE Inboard	9.547	-	10.08	-	-
LE	11.37	11.74	-	8.82	-
			Control Rates (deg/sec)		
TE Outboard	-	145.7	144.1	-	157.7
TE Inboard	133.9	-	132.4	-	-
LE	148.4	145.9	-	180.1	-
			Bending Moment (inch-lbs)		
	15120	19500	19290	20700	23960
			Shear (lbs)		
	352.1	487.6	502.2	404.5	516.7
			Torque (inch-lbs)		
	922.4	1146	2868	1939	1896
			Minimum Singular Value		
	0.531	0.649	0.681	0.242	0.580

Table 7: Effects of a Single Control Failure on Final Full State Designs

Section 5

Loop Transfer Recovery

After the full state feedback regulator gains K are designed, the state estimator gains L are determined using the LTR method described in section 3.2. This method requires a square system. Four sensors (accelerometers) are available as shown in Fig. 1. The sensors closest to the control surfaces are the ones chosen for use in the system. Thus, the three-control system uses sensors 2, 3, and 4, and the two-control system uses sensors 3 and 4.

The transmission zeros and left zero directions of the plant are found by using the EISPACK routine RGG, which solves the generalized eigenvalue problem $(\lambda_i \mathbf{B}-\mathbf{A})x_i=0$. By letting

$$\mathbf{A} = \begin{bmatrix} A^T & -C^T \\ B^T & 0 \end{bmatrix} \qquad \mathbf{B} = \begin{bmatrix} I & 0 \\ 0 & 0 \end{bmatrix}$$

$\lambda_i = z_i$, and $x_i^T = [\mu_i^T \; \zeta_i^T]$, RGG is made to solve Eq. 17. for z_i and μ_i. The transmission zeros thus found fall into three distinct groups. Most are well behaved, with magnitudes comparable to the magnitudes of the eigenvalues of the system, but some have very large magnitudes, while others have very small magnitudes in comparison with the system eigenvalues. Since the small magnitude zeros arise from the double differentiations resulting from each accelerometer, these zeros should lie exactly on the origin. There are six such zeros in the three-control case and four in the two-control case.

Some of the very large and very small magnitude transmission zeros returned by the computer fall into the right half plane. This is caused by the errors introduced by finite precision arithmetic. RGG returns the zeros in the fractional form $(\propto_{real}+j\propto_{imag})/\beta$. For the accelerometer zeros, a small error in $\propto_{real}$ can cause the zero to shift away from the origin and into the right half plane. In the case of a large magnitude zero, where $\beta \approx 0$, a small error in β can change its sign, sending the transmission zero into the right half plane.

Fig. 7 shows the transmission zeros found above as well as the open loop estimator eigenvalues for the three-control case. In order to keep the magnitude of the estimator gains small, the open loop estimator eigenvalues are assigned to the closest transmission zeros. Estimator eigenvalues corresponding to structural modes 4 and 9, gust modes, and unsteady aerodynamic modes are driven to nearby transmission zeros. The

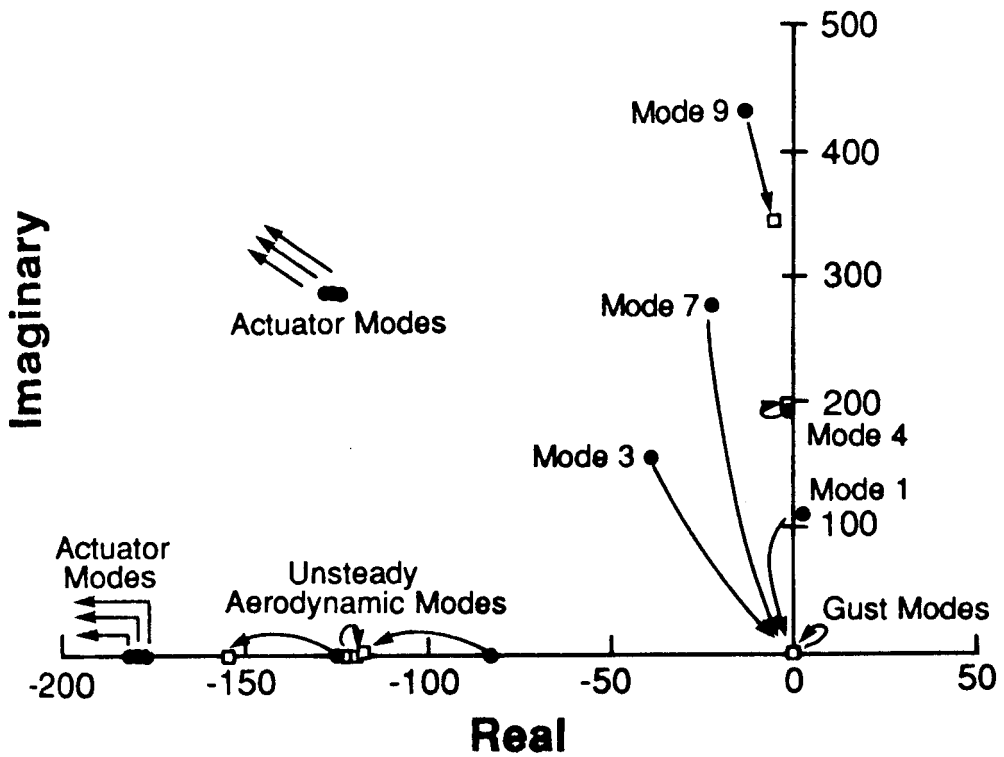

Figure 7: Estimator Poles and Open Loop Transmission Zeros for Three-Control Case

estimator eigenvalues associated with the actuators are sent to the large magnitude transmission zeros, and are referred to here as "infinity" poles. In the three-control case, the six remaining eigenvalues (three complex conjugate pairs) corresponding to structural modes 1, 3, and 7 are sent to the six transmission zeros near the origin. These are termed "zero" poles. The two-control case is similar to the three-control case except that mode 7 is driven to a nearby pair of finite zeros which appear instead of one of the accelerometer pairs. For "zero" and 'infinity" transmission zeros which are in the right half plane, left half plane mirror images are used instead to provide for a stable system.

By the separation principle, the set of eigenvalues of the combined estimator/regulator is the union of the eigenvalues of A-LC and A+BK. While the software was sufficient for the 26th order regulator design, it had difficulty with the 52nd order system formed by the regulator/estimator. In addition to its size, the system which results from the placement of estimator eigenvalues and eigenvectors as described above has eigenvalues which span 15 orders of magnitude. It is also ill-conditioned since the zero poles are nearly equal. The computed closed loop eigenvalues of this 52nd order system are entirely unlike those of A-LC and A+BK, and the estimator gains are incredibly large. Setting the zero poles identically equal to zero does not improve the situation. By moving the estimator zero poles and infinity poles as described below, more reasonable results are obtained.

Another numeric problem arises in the two-control case: a pair of the transmission zeros near the origin are real and reflexive (i.e. $z_1=-z_2$). When used as estimator poles, the two form a multiple pole since the positive real zero is negated to place it in the left-half plane. Multiple poles typically create problems for eigenvalue software, hence the poles are shifted slightly to separate them. The interesting result is that this reduces bending moment, torque, and control deflections by an order of magnitude, indicating extreme sensitivity to the placement of these poles.

Before testing the effects of moving the zero poles and infinity poles, a 52nd order base case which the software can handle is established. The magnitudes of the infinity poles are reduced to 880, which is about twice as large as the largest finite pole. This is defined as unity scaling for the infinity poles. Zero pole magnitudes are increased by simply dropping the exponent of the scientific notation of the zero poles. For example, $-1.3\times10^{-2}\pm j4.3\times10^{-3}$ becomes $-1.3\pm j4.3$. The resulting set of zero poles are designated as having a zero pole scaling of one.

Holding the infinity pole scaling at unity, the effects of moving the zero poles by changing the zero pole scaling are shown in Figs. 8 and 9. Decreasing the zero pole scaling, which places the zero poles closer to the origin, causes an increase in bending moment, torque, and control deflection rms. Bending moment actually has a minimum at a zero pole

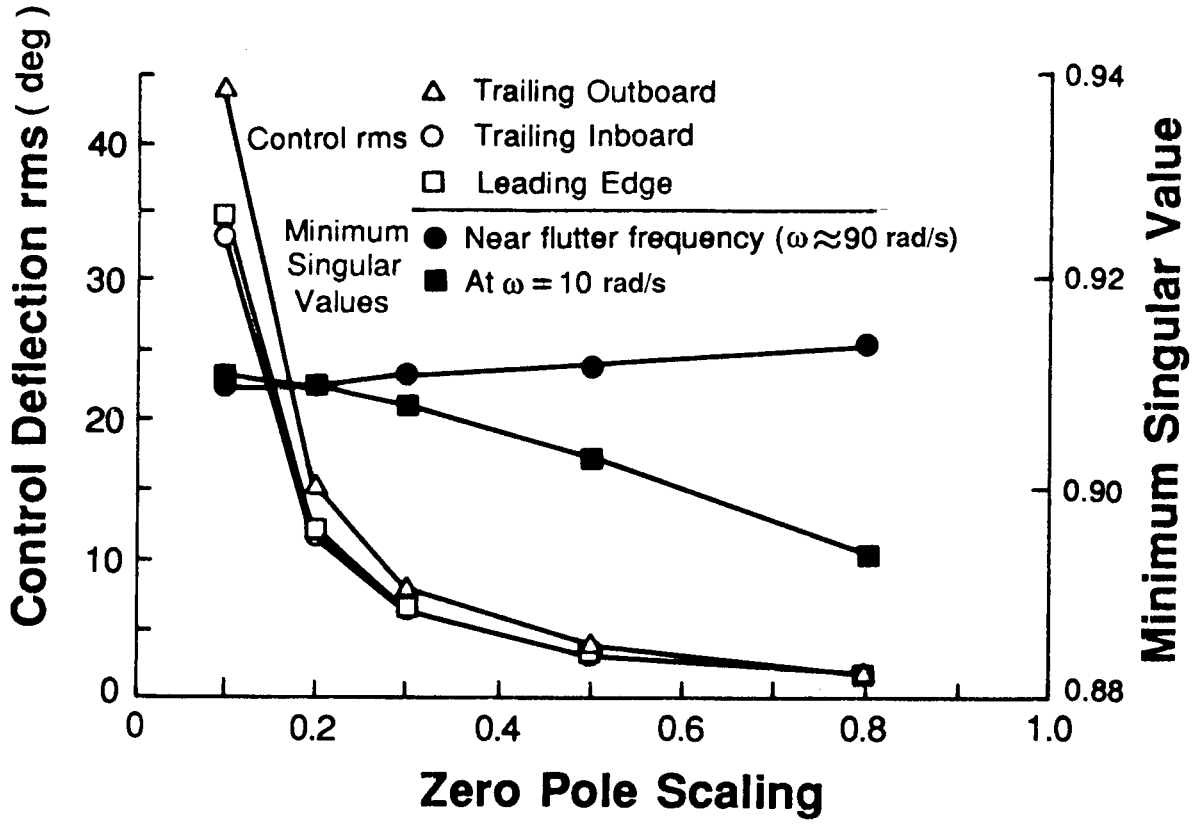

Figure 8: Effect of Zero Estimator Pole Location on Minimum Singular Value and Control Effort

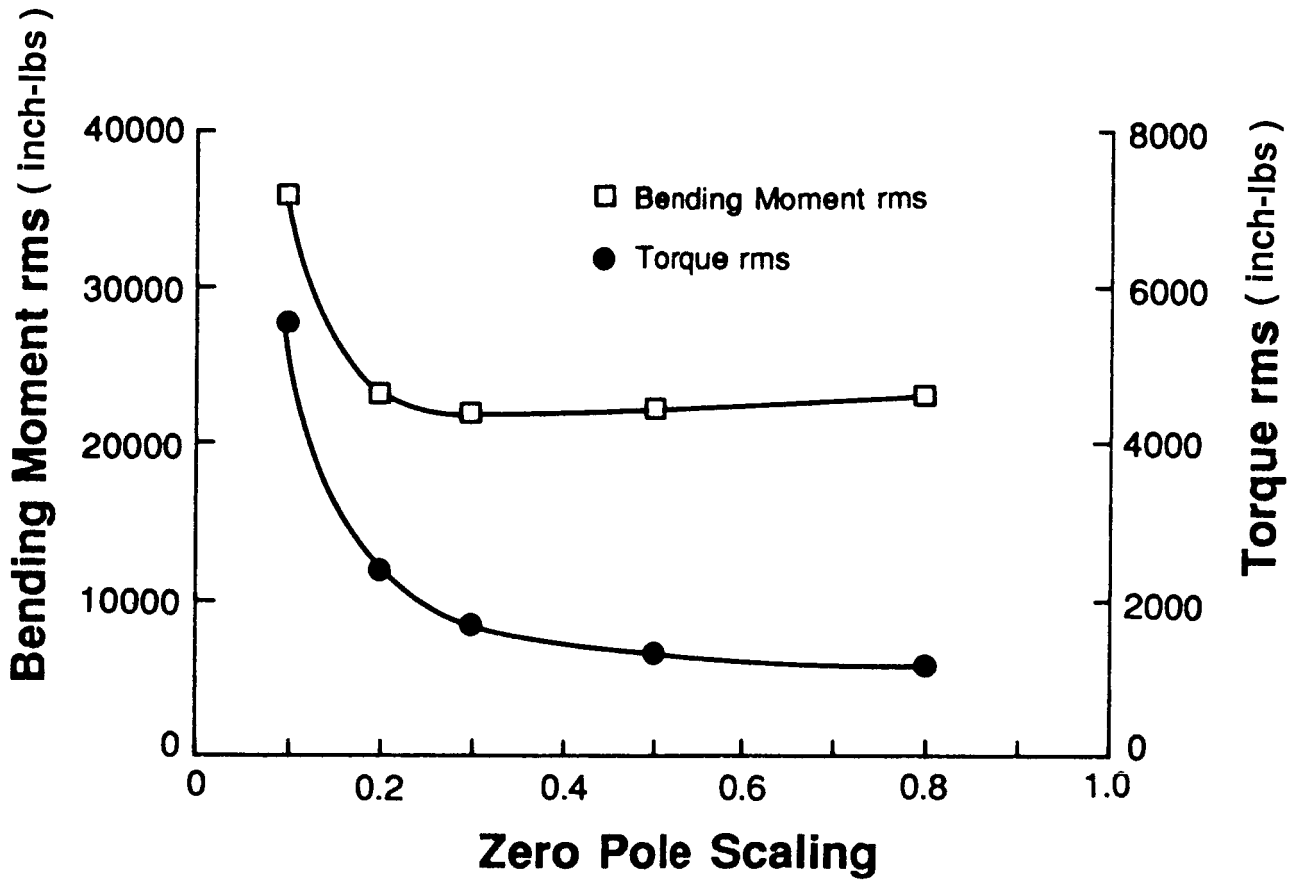

Figure 9: Effect of Zero Estimator Pole Location on Bending Moment and Torque

scaling of 0.3. For a zero pole scaling less than 0.3, these quantities increase rapidly. Minimum singular values of the return difference matrix are given for both $\omega = 10$ and $\omega \approx 90$ rad/sec in Fig. 8 because, as shown in Fig. 12, the minimum singular value achieves minima near these two frequencies. As the zero poles approach the origin, the minimum singular value at $\omega \approx 90$ rad/sec decreases slightly, while the minimum singluar value at $\omega = 10$ rad/sec increases. The zero poles corresponding to a zero pole scaling of 0.3 are chosen for the final design to obtain good minimum singular values without control saturation or excessive wing root loads.

Fixing the zero pole scaling at 0.3, the infinity pole scaling is similarly adjusted. In Figs. 10 and 11 it is shown that increasing the magnitude of the infinity poles reduces bending moment, torque, and control rms, while it increases the minimum singular values at both $\omega = 10$ and $\omega \approx 90$ rad/sec. The estimator feedback gains increase by approximately one order of magnitude for each step shown in Figs. 10 and 11. An infinity pole scaling of five is chosen since larger scalings do not yield significantly better performance or robustness. As expected, varying the weightings for the estimator eigenvectors corresponding to the estimator infinity poles has no effect on the behavior of the system since these eigenvectors are arbitrary.

As can be seen in Figs. 8-11, the locations of the zero poles of the estimator have a greater affect on both the rms responses and the singular values than do the locations of the estimator infinity poles. With the Doyle-Stein approach to LTR, all estimator poles move simultaneously and it is not possible to evaluate the effects of independently varying the locations of the estimator zero and infinity poles.

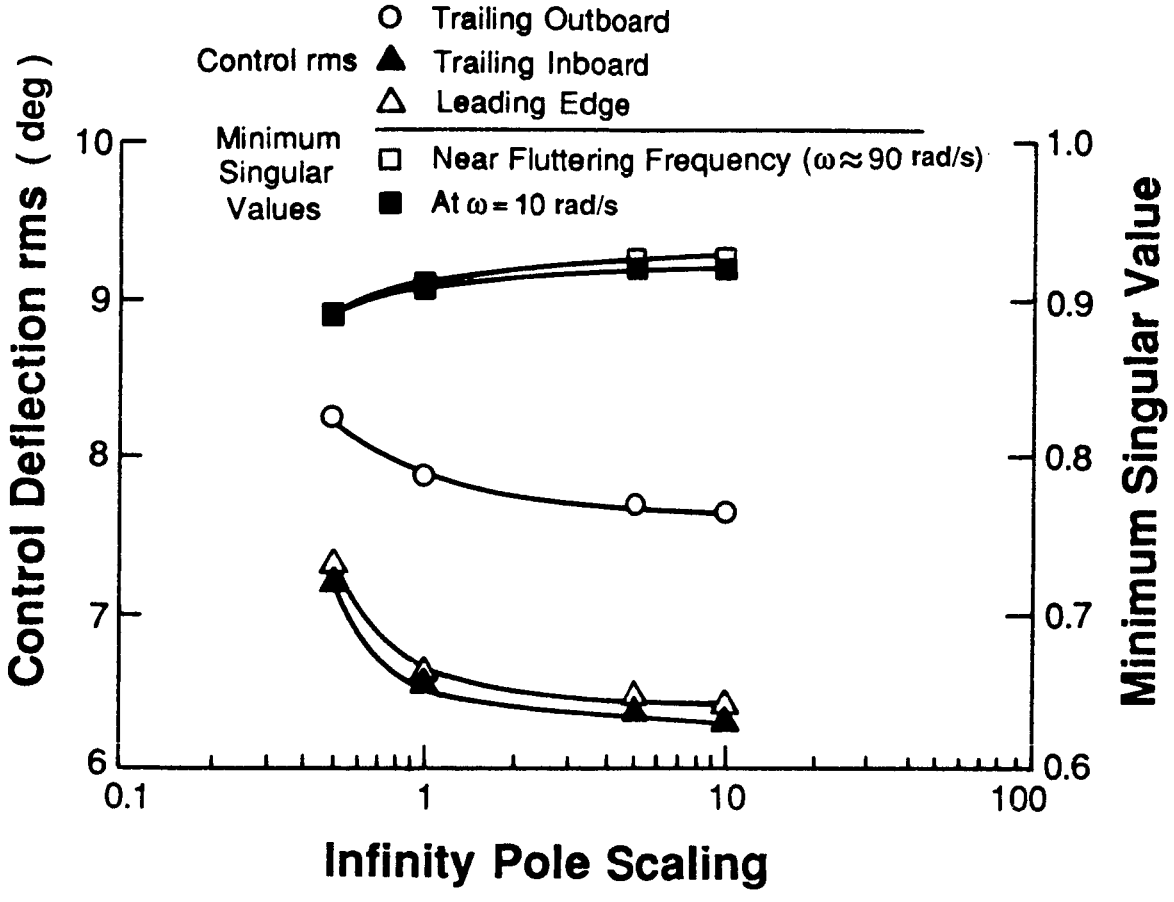

Figure 10: Effect of Infinite Estimator Pole Location on Minimum Singular Value and Control Effort

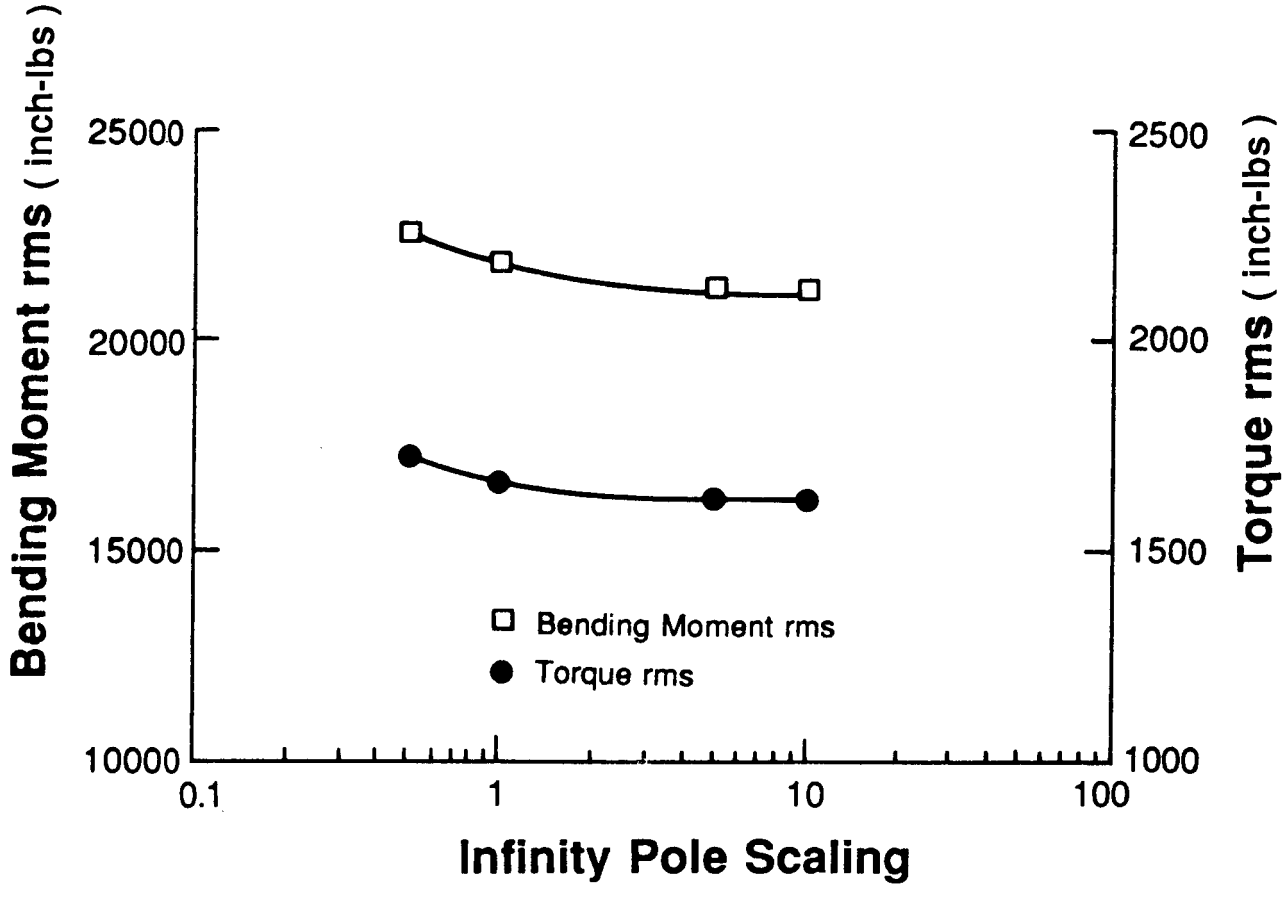

Figure 11: Effect of Infinite Estimator Pole Location on Bending Moment and Torque

Section 6

Final Designs

The results for the final regulator/estimator designs are summarized in Tables 8 and 9 and Figs. 12-14. The effects of sensor noise equal to 5% of full state regulator accelerometer outputs are included in Tables 8 and 9. Accelerometer bandwidth is 10,000 Hz. Comparing Tables 6 and 8 it can be seen that other than bending moment in the three-control case, the performance parameters (control activity, wing root loads, and singular values) have been nearly recovered. The three-control case still has a lower bending moment than the two-control case, though still at the expense of higher torque and lower stability margins. Both designs have good stability margins, and both have control rms deflections which are only about half of the saturation values. In both cases the bending moment at the design velocity is actually less than that of the open loop system at a lower velocity.

The gust load alleviation provided by the control systems at a velocity for which the wing is open loop stable is also shown in Table 8. The two-control case provides a 10% reduction in bending moment with no increase in torque, while the three-control case reduces bending moment 15%, though with a 40% increase in torque. In both cases shear changes very little and stability margins are good. Since the bending moment is an order of magnitude greater than the torque, a significant reduction in total wing root load is achieved. At no point are the control surfaces found to saturate.

Stabilization of the first bending mode at the design velocity is shown by the closed loop root locus in Fig. 13. The onset of flutter now occurs at a velocity of 941 fps. This is a 5% increase in flutter speed compared with the open loop configuration. In the previous study [22,23] with a different mathematical model of the wing, a 28% increase in flutter speed was achieved. In an attempt to increase the flutter speed for the wing used in this study, the real parts of the poles associated with the the unstable mode were moved still farther to the left. The results are shown in Table 10. In order to achieve a 17% increase in flutter speed, the real parts of these poles had to be moved to -200. With full state feedback the control surface activity was within acceptable bounds but with the compensator in place the control surface deflections exceeded the allowable limits. In this report the design point of 909 fps is very close to the flutter speed of 896 fps; whereas, in the previous example the design speed was also 909 fps but the flutter speed was 750 fps. This means that the wing was considerably less stiff in the previous example and it is felt that this difference in the mathematical models of the wing

	3-control	2-control	Open-loop	3-control	2-control
Velocity(fps)	909	909	833	833	833
		RMS Responses			
		Control Deflections (deg)			
TE Outboard	7.669	8.231	-	7.374	7.873
TE Inboard	6.366	-	-	6.092	-
LE	6.469	6.333	-	6.19	6.054
		Control Rates (deg/sec)			
TE Outboard	65.93	90.78	-	42.37	50.67
TE Inboard	55.98	-	-	33.48	-
LE	57.51	73.95	-	33.58	40.93
		Bending Moment (inch-lbs)			
	21310	22090	22980	19430	20640
		Shear (lbs)			
	464.3	466.2	412.1	420.1	428
		Torque (inch-lbs)			
	1632	1286	817.5	1141	813.3
		Minimum Singular Value			
	0.922	0.979	-	0.91	0.977
		MIMO Gain Margin (DB) $20\log(1/(1\pm MSV))$*			
	22,-5.7	33.6,-5.9	-	22,-5.7	38.4,-6
		MIMO Phase Margin (deg) $\pm\cos^{-1}(1-(MSV^2)/2)$			
	$\pm$54.9	$\pm$58.6	-	$\pm$54.9	$\pm$59.2

*MSV = Minimum Singular Value

Table 8: Performance of Final Compensator Designs

	3-control			2-control	
	Failed Control				
	TEO	TEI	LE	TEO	LE
	RMS Responses				
	Control Deflections (deg)				
TE Outboard	-	8.218	8.059	-	8.406
TE Inboard	5.968	-	6.157	-	-
LE	6.199	6.38	-	6.374	-
	Control Rates (deg/sec)				
TE Outboard	-	82.72	81.6	-	131.
TE Inboard	82.43	-	72.14	-	-
LE	83.41	73.93	-	173.9	-
	Minimum Singular Value				
	0.527	0.644	0.679	0.293	0.583
	MIMO Gain Margin (DB) 20 log(1/(1±MSV))*				
	6.5,-3.7	9.0,-4.3	9.9,-4.0	3.0,-2.2	7.6,-4.0
	MIMO Phase Margin (deg) $\pm\cos^{-1}(1-(MSV^2)/2)$				
	±30.6	±37.6	±39.6	±16.8	±33.9

*MSV = Minimum Singular Value

Table 9: Effects of a Single Control Failure on Final Compensator Designs

	-8.1*	-40*	-80*	-200*	-40**	-200**
Mode 1 Pole Position (Real Part)						
RMS Control Responses						
Control Deflections (deg)						
TE Outboard	12.09	12.1	12.1	12.1	18.6†	24.1†
TE Inboard	10.44	10.46	10.47	10.48	22.48†	60.43†
LE	11.77	11.78	11.77	11.76	17.65†	29.9†
Control Rates (deg/sec)						
TE Outboard	136.2	135.8	137.4	150.7	134.8	305.5
TE Inboard	125.7	130.8	137.4	151.5	87.44	159.0
LE	138.4	137.8	133.8	138.9	94.29	253.8

RMS Structural Responses*

(Full state responses were constant to within a few percent.)

Bending Moment (inch-lbs)	14660
Shear (lbs)	446
Torque (inch-lbs)	1962

Minimum Singular Value					
0.93	0.947	0.962	0.952	0.915	0.9
Flutter Velocity (fps)					
941	987	1011	1052	†	†
Flutter Velocity Increase (%)					
5	10	13	17	†	†

* Full State Regulator

** Regulator/Estimator

† Control Saturation

Table 10: Effects of Mode 1 Pole Placement

structures used in the two studies accounts for the difficulty in achieving as large a percentage increase in the flutter speed. It should be noted that the absolute closed loop flutter speed was 941 fps in this study whereas in the previous example it was 960 fps, a difference of only 2%.

Fig. 12 clearly shows the loop transfer recovery by plotting the minimum singular value of the return difference matrix versus frequency for the two- and three-control systems with full state feedback and with estimators in the feedback loops. As in the full state feedback case, the two-control system has higher minimum singular values, making it the more robust system. Recovery is best near the flutter frequency, but is also good at low and high frequencies as well.

Minimum singular values for the two- and three-control systems are plotted versus velocity in Fig. 14. The minimum singular values peak at the design velocity, hence the systems are most robust at this velocity. Above the design velocity the system rapidly loses robustness, becoming unstable near 941 fps (4.61 psi) as the eigenvalues of the first bending mode move into the right-half plane. At lower velocities the singular value is somewhat reduced but never falls below 0.9 for the two-control case and 0.8 for the three-control case. Thus the flutter control system does not cause the wing to become unstable at velocities where it is open loop stable.

The effects of a single, undetected control surface failure are examined for the final regulator/estimator designs. In Table 9 it can be seen that though the loss of any one control surface reduces the minimum singular value and increases control surface rms, no control surface saturates and the designs are still nominally stable. Even the worst case, the failure of the TE outboard surface in the two-control case, MIMO gain margins of +3.0 and -2.2 DB and MIMO phase margins of ±16.8 degrees are maintained.

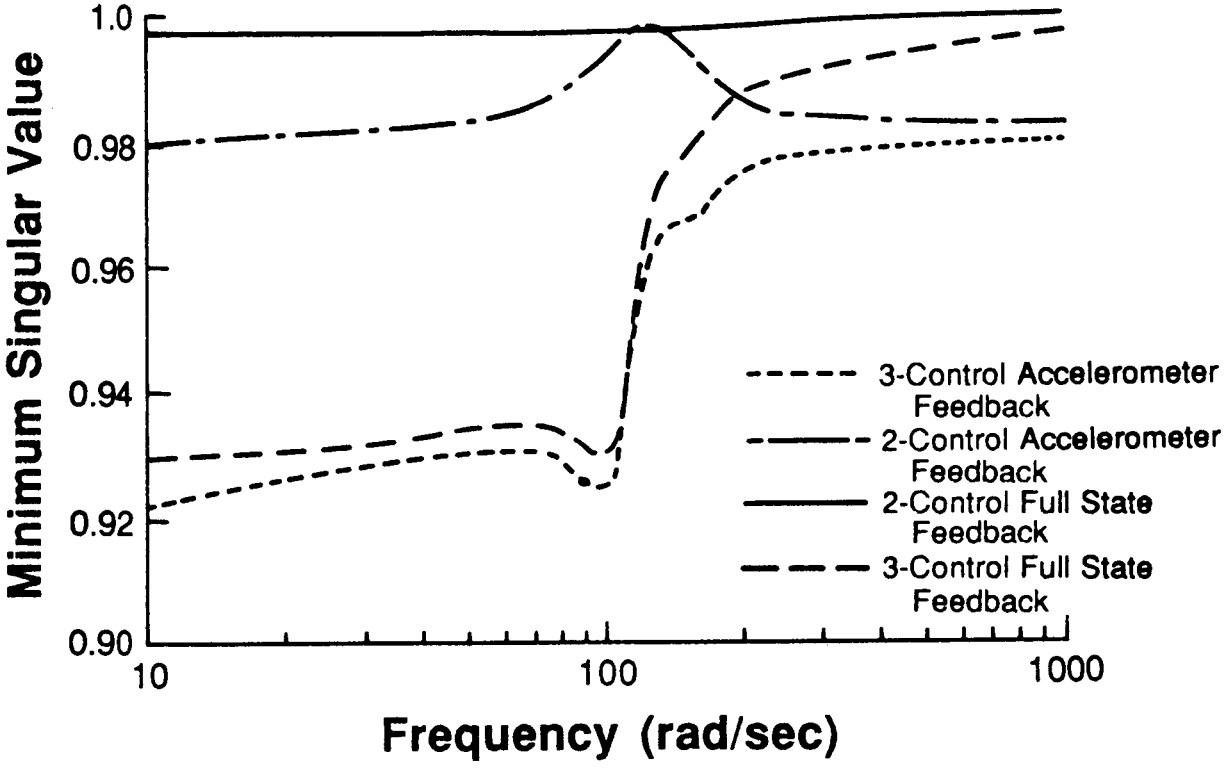

Figure 12: Minimum Singular Values of the Return Difference Matrices versus Frequency

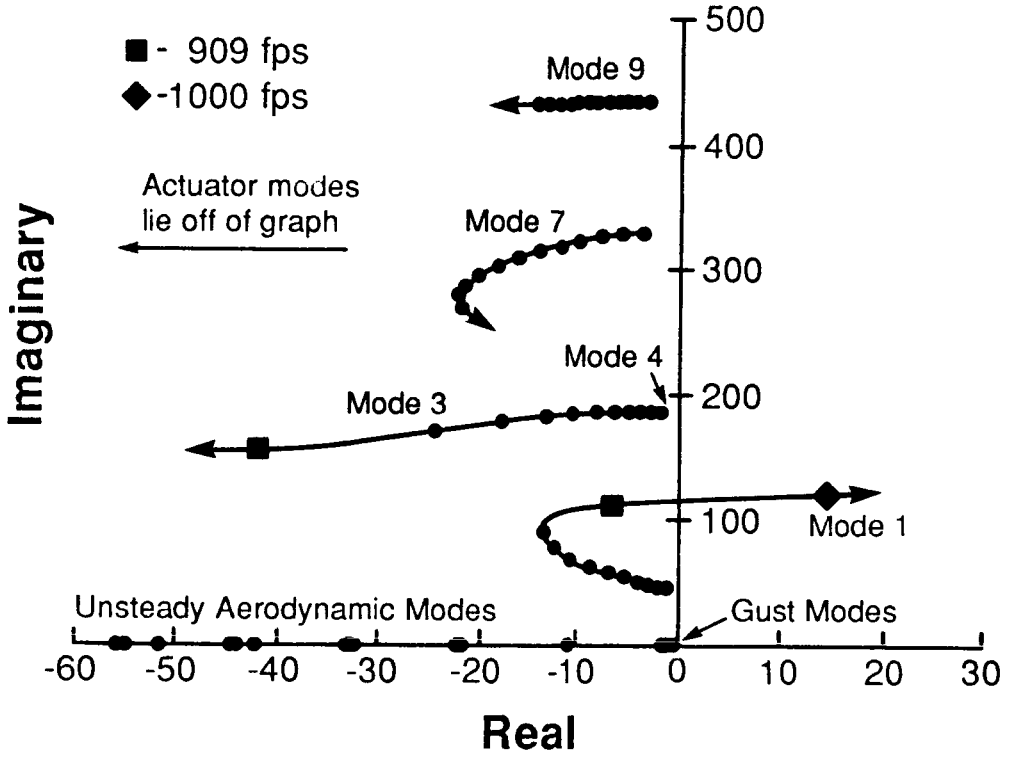

Figure 13: Locus of Closed Loop Aeroelastic Roots with Velocity

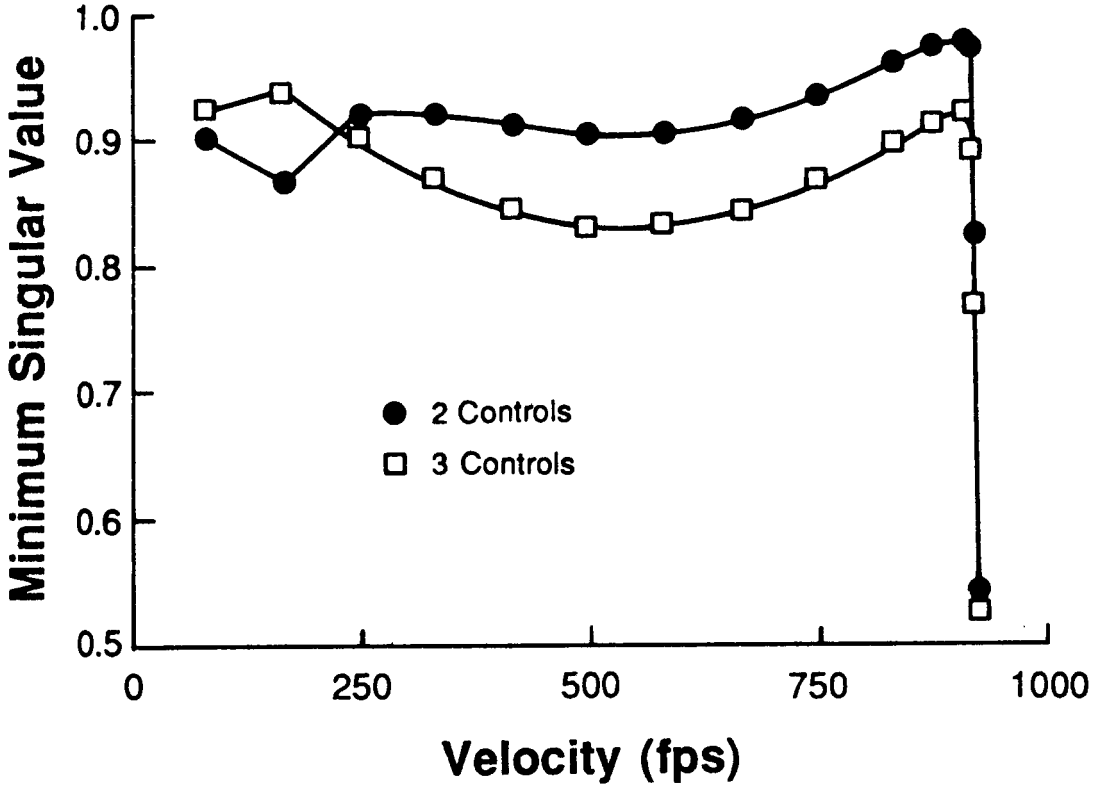

Figure 14: Minimum Singular Values of the Return Difference Matrices versus Velocity

SECTION 7

CONCLUSIONS

In this report a complete theory for eigenspace design of control laws and state estimators is presented which is analogous to full state control design via LQR theory, estimator design via Kalman filter theory, and LTR via the Doyle-Stein techniques. This eigenspace theory is successfully applied to the design of an active flutter suppression/gust load alleviation system for a hypothetical model of a wing with leading and trailing edge control surfaces. Robust flutter stabilization is achieved by eigenvalue placement, and wing root loads are reduced by eigenvector shaping. The full state regulator properties are then recovered by direct placement of estimator eigenvalues and eigenvectors at or near the plant transmission zeros and associated left zero-directions.

In aircraft control problems in which performance specifications are specified or can be easily interpreted in terms of eigenvalue/eigenvector placements (i.e. handling qualities enhancement, modal decoupling) eigenspace techniques appear to be the most efficient approach to control law design. In other situations such as many aeroelastic control problems, where the order of the system is high and the desired closed loop eigenstructure is not apparent, it may be necessary to perform a number of iterations on the desired closed loop eigenstructure before acceptable performance is achieved. Thus in these cases the design procedure is not much different from LQG design using the Doyle-Stein technique for LTR in which a number of iterations are made until acceptable performance is achieved. Both eigenspace and LQG techniques usually involve trading off rms responses and LTR, however, eigenspace LTR offers the additional flexibility over Doyle-Stein LTR of being able to independently move finite and infinite estimator poles.

In systems in which leading and trailing edge surfaces are used it is important that control effort should be balanced between the leading and trailing edge to provide bending moment reduction without an increase in torque.

Section 8

REFERENCES

1. Cunningham, Thomas B., "Eigenspace Selection Procedures for Closed Loop Response Shaping With Modal Control," Proceedings 19th IEEE Conference on Decision and Control, Dec. 1980, pp 178-186.
2. Andry, A. N., Shapiro, E. Y., and Chung, J. C., "Eigenstructure Assignment for Linear Systems," IEEE Trans. on Aerospace Electronic Systems, Sept. 1983, Vol AES-19, pp 711-729.
3. Sobel, K. M., and Shapiro, E. Y., "Application of Eigenspace Assignment to Lateral Translation and Yaw Pointing Flight Control," Proceedings 23rd IEEE Conference on Decision and Control, Dec. 1984, pp 1423-1438.
4. Sobel, K. M., and Shapiro, E. Y., "A Design Methodology for Pitch Pointing Flight Control Systems," J. of Guidance, Control and Dynamics, Vol 8, March-April 1985, pp 181-187.
5. Ostroff, A. J., and Pines, S., "Application of Modal Control to Wing-Flutter Suppression," NASA TP-1983, May 1982.
6. Alag, G. S., Burken, J. J., Gilyard, G. B., "Eigensystem Synthesis for Active Flutter Suppression on an Oblique-Wing Aircraft," Proceedings 1986 AIAA Guidance and Control Conference, August 1986.
7. Shomber, Henry A., "Application of Integrated Active Controls to Future Transports," AIAA Paper 79-1654, Proceedings 1979 Guidance and Control Conference, August 1979.
8. Murrow, H. N., and Eckstrom, C. V., "Drones for Aerodynamic and Structural Testing (DAST)- A Status Report," AIAA Paper 18-1485, 1978 Atmospheric Flight Mechanics Conference, August 1978.
9. Abel, I., Perry, B., and Murrow, H. N., "Two Synthesis Techniques Applied to Flutter Suppression on a Flight Research Wing," J. of Guidance and Control, Vol 1, Sept.-Oct. 1978, pp 340-346.
10. Visor, O. E., and Sevart, F. D., "Preliminary Design Study of Flutter Suppression Control System for the BQM-34/F Drone Aircraft with a Supercritical Wing - Final Report," NASA CR-145208, 1976.
11. Nissim, E., "Comparative Study Between Two Different Active Flutter Suppression Systems," J. of Aircraft, Vol 15, Dec.1978, pp 843-848.
12. Newsom, J. R., "Control Law Synthesis Using Optimal Control Theory," J. of Guidance and Control, Vol 2, Sept.-Oct. 1979, pp 388-394.
13. Abel, I., Newsom, J. R., and Dunn, H. J., "Application of Two Synthesis Techniques for Active Flutter Suppression of an Aeroelastic Wind Tunnel Model," AIAA Paper 79-1633, Aug. 1979.

14. Mahesh, J. K., Stone, C. R., Garrard, W. L., and Dunn, H. J., "Control Law Synthesis for Flutter Suppression Using Linear Quadratic Control Theory," J. of Guidance and Control, Vol 4, July-Aug 1981, pp 415-422.
15. Garrard, W. L., Mahesh, J. K., Stone, C. R., and Dunn, H. J., "Robust Kalman Filter Design for Active Flutter Suppression," J. of Guidance, Control and Dynamics, Vol 5, July-Aug 1982, pp 412-414.
16. Doyle, J. C., and Stein, G., "Multivariable Feedback Design: Concepts for a Classical/Modern Synthesis," IEEE Trans. on Auto. Control, Vol 26, Feb. 1981, pp 4-16.
17. Mukhopadhyay, V., Newsom, J. R., and Dunn, H. J., "Reduced Order Optimal Feedback Control Law Synthesis for Flutter Suppression," J. of Guidance and Control, Vol 4, July-Aug. 1981, pp 382-395.
18. Newsom, J. R., "Design of the Flutter Suppression System for a Remotely Piloted Research Vehicle (DAST ARW-1R)," AIAA Paper 83-0990-CP, Proceedings of the AIAA/ASME/ASCE/AHS Structures, Structural Dynamics, and Materials Conference, May 1983.
19. Schmidt, D. K., and Chen, T. K., "Frequency Domain Synthesis of a Robust Flutter Suppression Control Law," J. of Guidance, Control, and Dynamics, Vol 9, May-June 1986, pp 346-351.
20. Adams, W. M., and Tiffany, S. H., "Design of a Candidate Flutter Suppression Control Law for DAST ARW-2," NASA TM-86257, July, 1984.
21. Takahashi, M., and Slater, G. L., "Design of a Flutter Mode Controller Using Positive Real Feedback," J. of Guidance, Control and Dynamics, Vol 9, May-June 1986, pp 339-345.
22. Garrard, W. L., and Liebst, B. S., "Active Flutter Suppression Using Eigenspace and Linear Quadratic Design Techniques," J. of Guidance, Control and Dynamics, Vol 8, May-June 1985, pp 304-311.
23. Liebst, B. S., Garrard, W. L., and Adams, W. M., "Design of an Active Flutter Suppression System," J. of Guidance, Control and Dynamics, Vol 8, Jan-Feb 1986, pp 64-71.
24. Moore, B. C., "On the Flexibility Offered by Full State Feedback In Multivariable Systems Beyond Closed Loop Eigenvalue Assignment," IEEE Trans. on Auto. Control, Vol 21, Oct. 1976, pp 682-691.
25. Harvey, C. A., and Stein, G., "Quadratic Weights for Asymptotic Regulator Properties," IEEE Trans. on Auto. Control, Vol 23, June 1978, pp 378-381.
26. Stein, G., "Generalized Quadratic Weights for for Asymptotic Regulator Properties," IEEE Trans. on Auto. Control, Vol 24, Aug. 1979, pp 559-566.
27. Safanov, M. G., and Athans, M., "Gain and Phase Margins of Multiloop Regulators," IEEE Trans. on Auto. Control, Vol 22, April 1977, pp 173-179.
28. Gilbert, E. G., "Conditions for Minimizing Norm Sensitivity of Characteristics Roots," IEEE Trans. on Auto. Control, Vol 29, Aug 1984, pp 623-626.

29. Kazerooni, H., and Houpt, P. K., "On the Loop Transfer Recovery," Int. Journal of Control, Vol 43, 1986, pp 981-996.
30. Dowell, E. H., "A Simple Method for Converting Frequency-Domain Aerodynamics to the Time Domain," NASA TM-81844, Oct. 1980.
31. Kwakernaak, H., and Sivan, R., Linear Optimal Control Systems, Joaahn Wiley, 1972.
32. Safonov, M. G., Laub, A. J., and Hartmann, G. L., "Feedback Properties of Multivariable Systems: The Role and Use of the Return Difference Matrix," IEEE Trans. on Auto. Control, Vol 26, Feb. 1981, pp 47-65.
33. Lehtomaki, N. A., Sandell, N. R., and Athans, M.,"Robustness Results in Linear Quadratic Based Multivariable Controller Design," IEEE Trans. on Auto. Control, Vol 26, Feb. 1981, pp 75-92.

Appendix

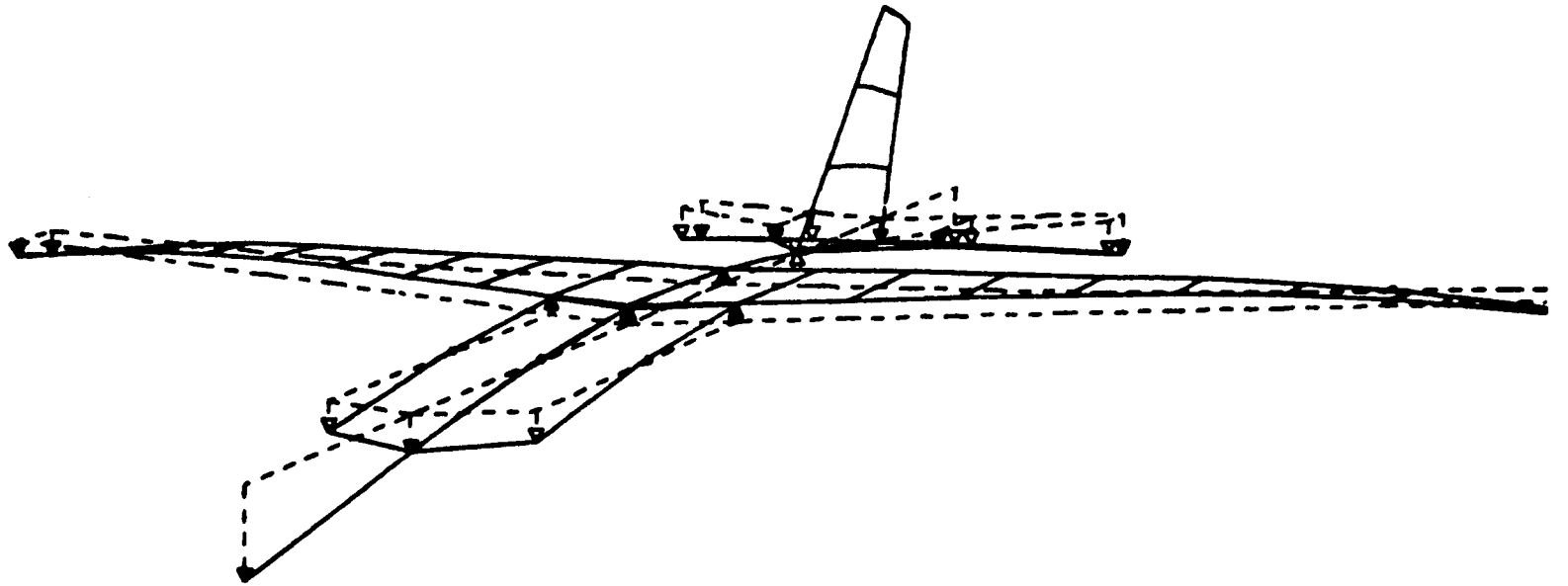

AREALS2.PL.XMT=313.75=XVT.197MODE= 2. FREQ= 14.89HZ. GMASS= 0.

ACPO

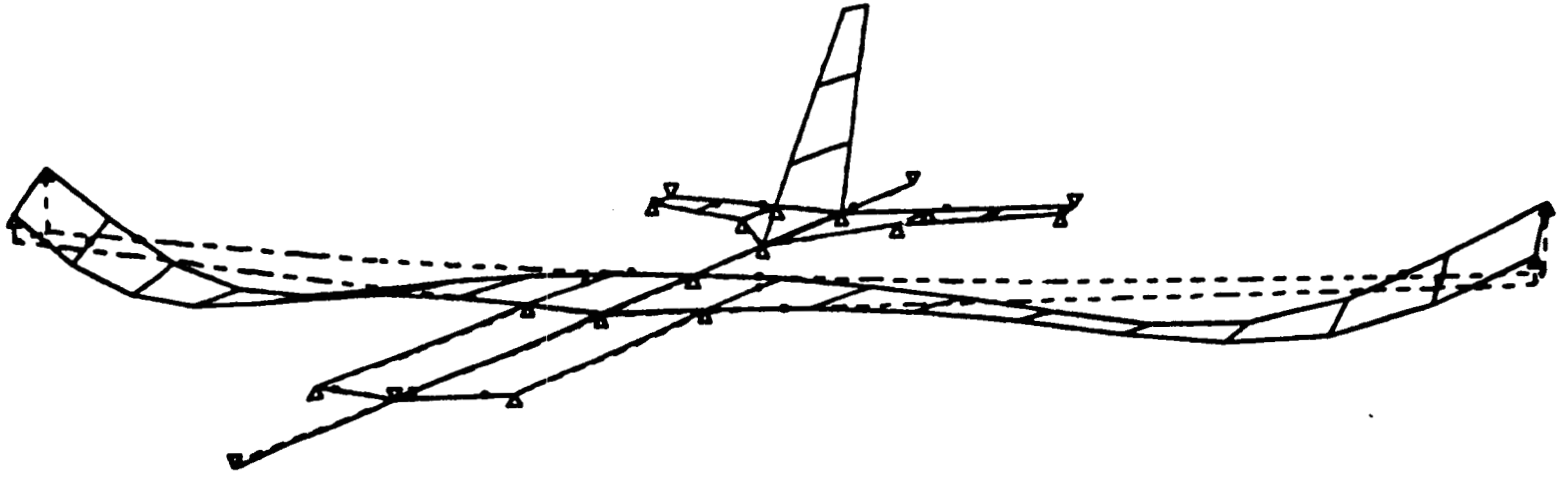

AREALS2.PL.XHT=319.75=XVT.197MODE= 3. FREQ= 29.54HZ. GMASS= 0.

ACPO

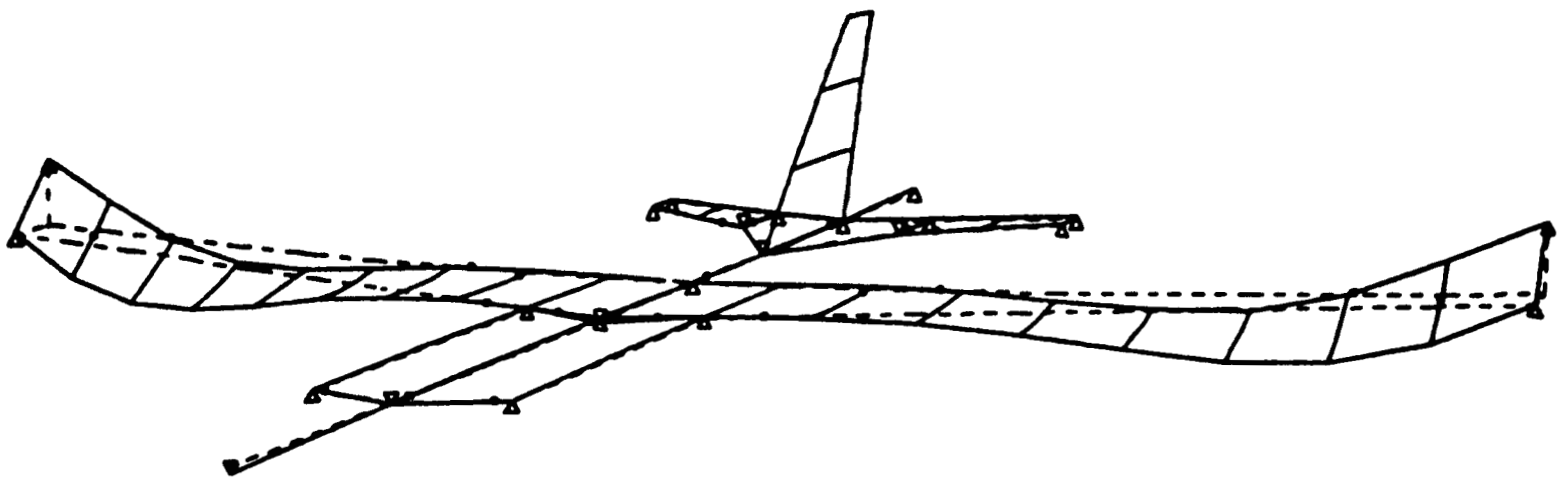

AREALS2.PL.XHT=319.75=XVT.197MODE= 4. FREQ= 31.45HZ. GMASS= 0.

ACPO

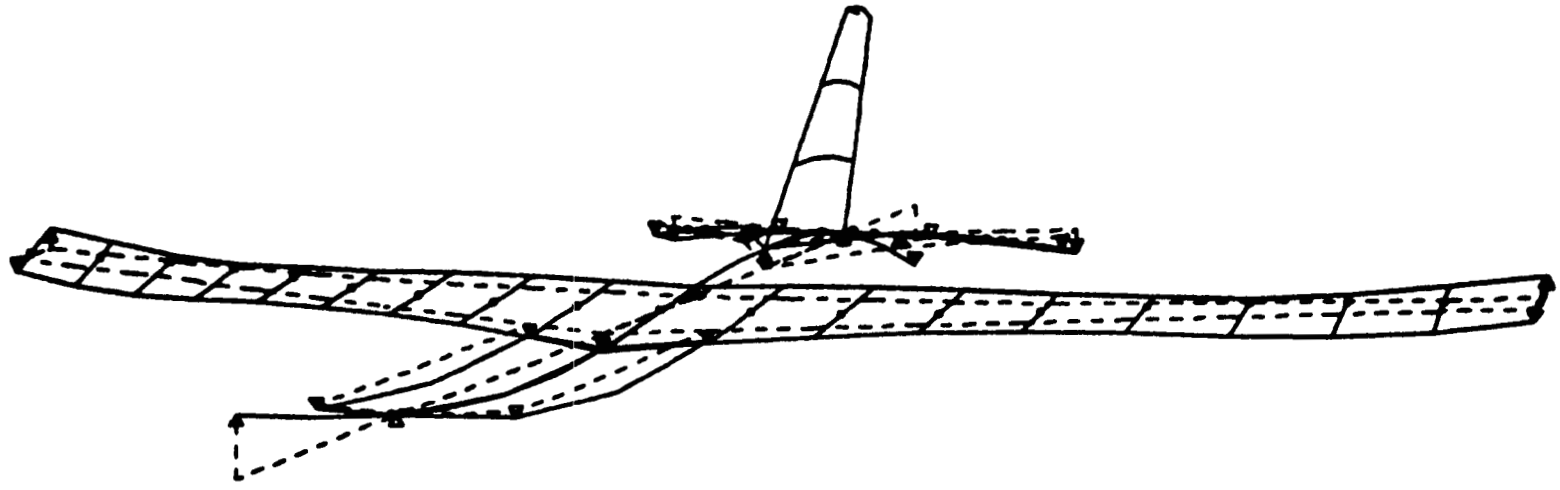

AREAL52.PL.XHT=313.75=XVT.197MODE= 5. FREQ= 37.18HZ. GMASS= 0.

ACPO

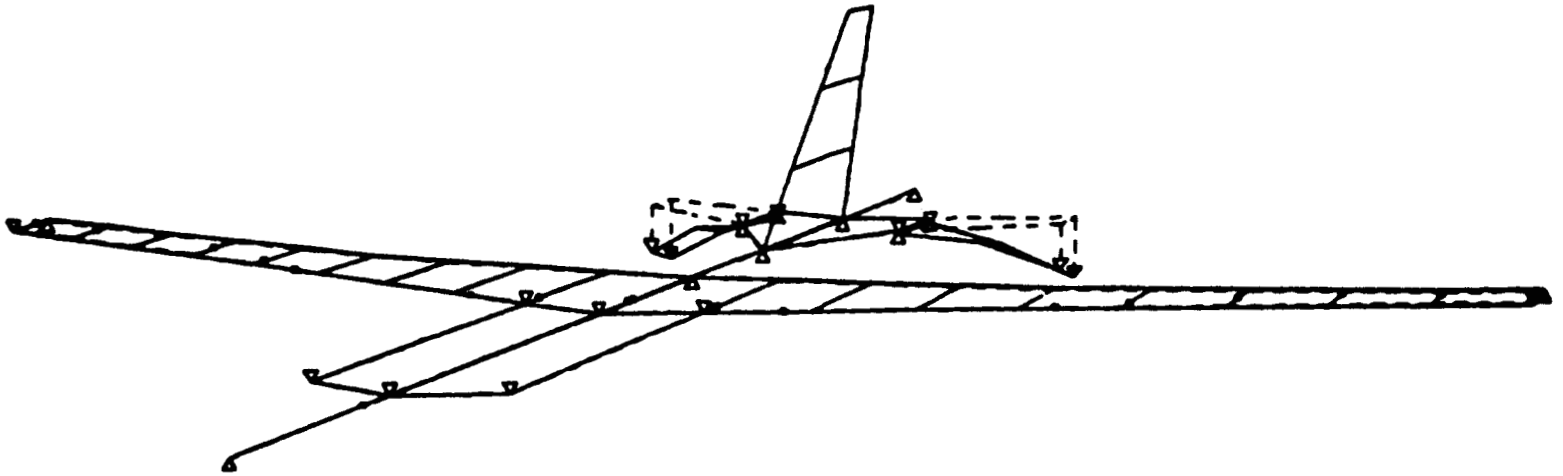

AREALS2.PL.XHT=313.75=XVT.197MODE= 6. FREQ= 50.24HZ. GMASS= 0.

ACPO

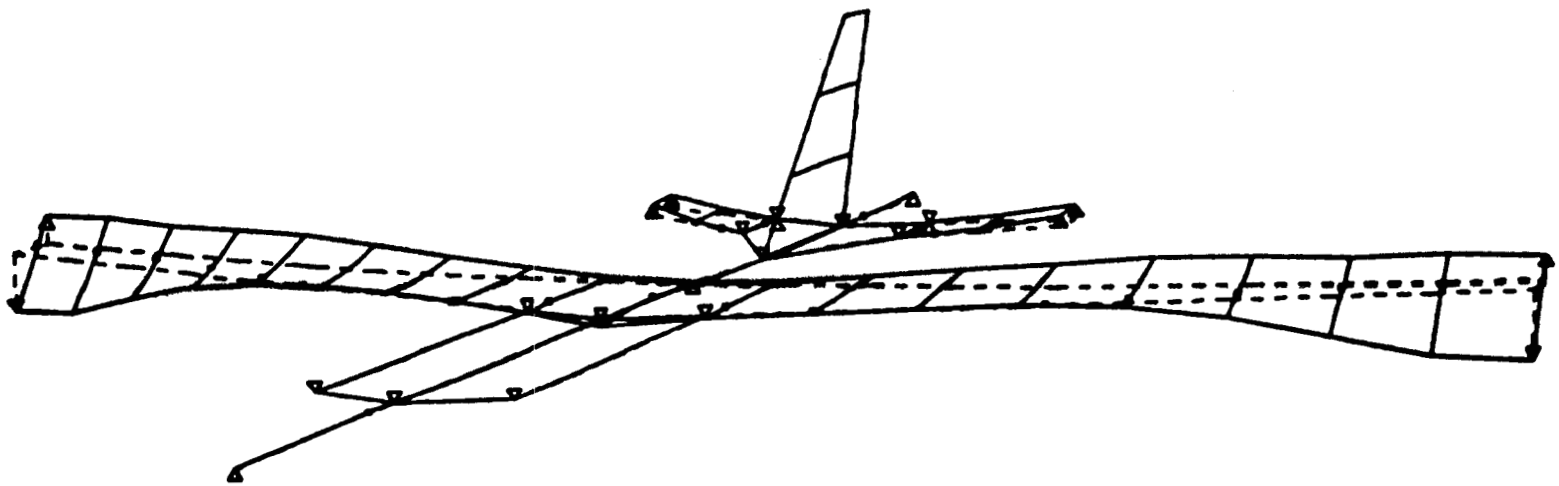

AREALS2.PL.XHT=313.75=XVT.197MODE= 7. FREQ= 51.90HZ. GMASS= 0.

ACPO

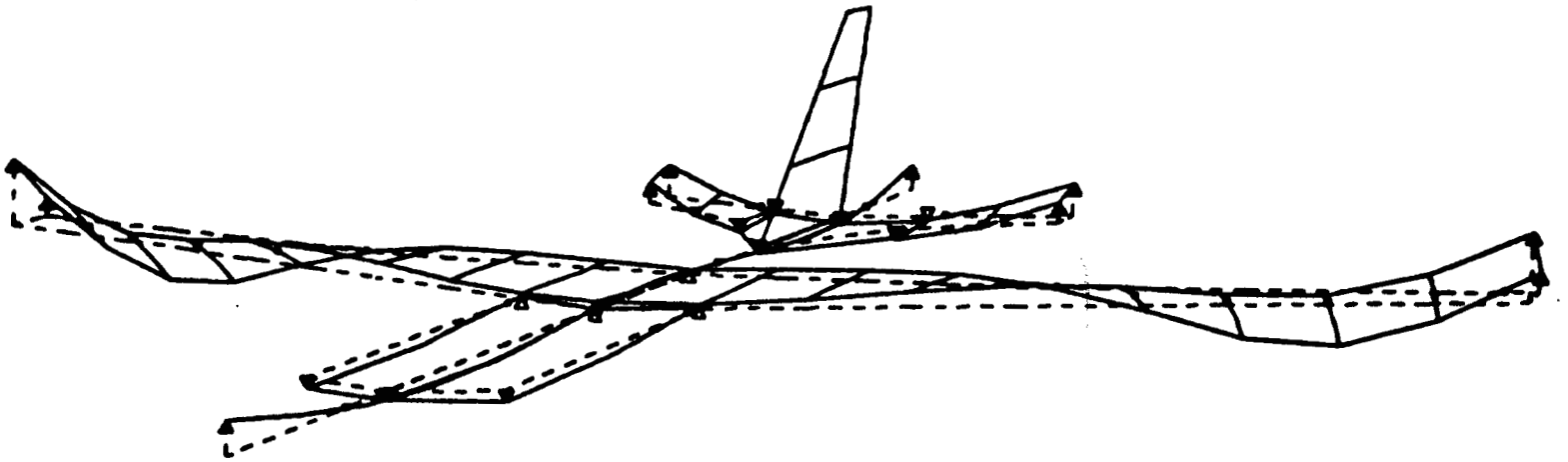

AREALS2.PL,XHT=313.75=XVT,197MODE= 8, FREQ= 62.85HZ, GMASS= 0.

ACPO

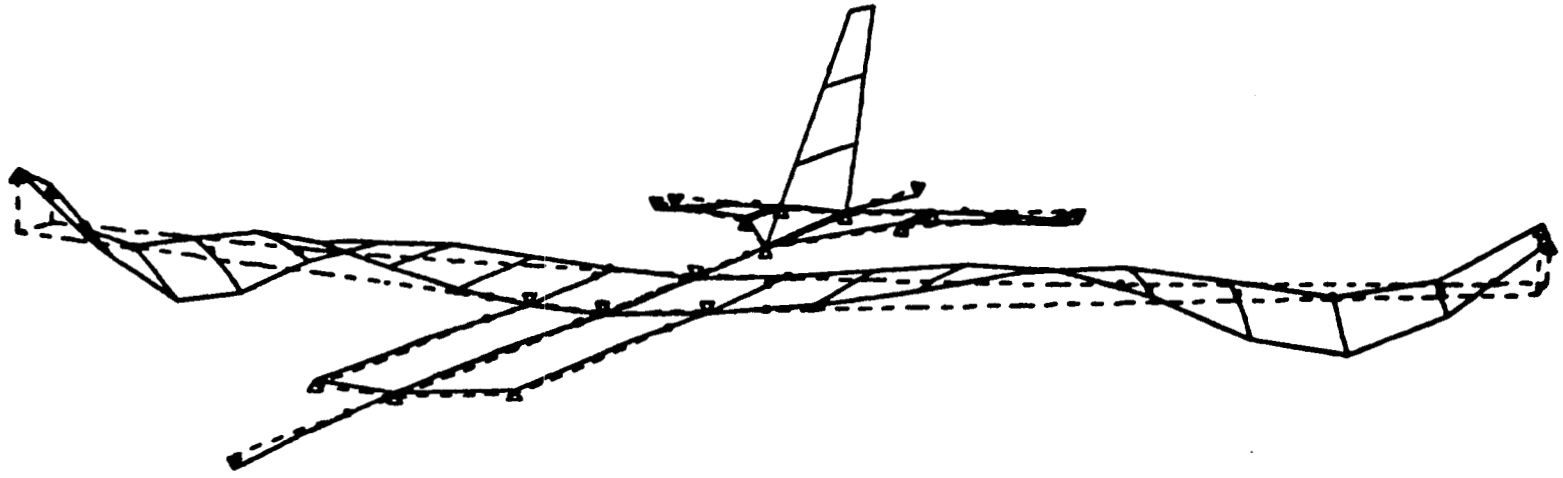

AREALS2.PL.XHT=313.75=XVT.197MODE= 9. FREQ= 69.13HZ. GMASS= 0.

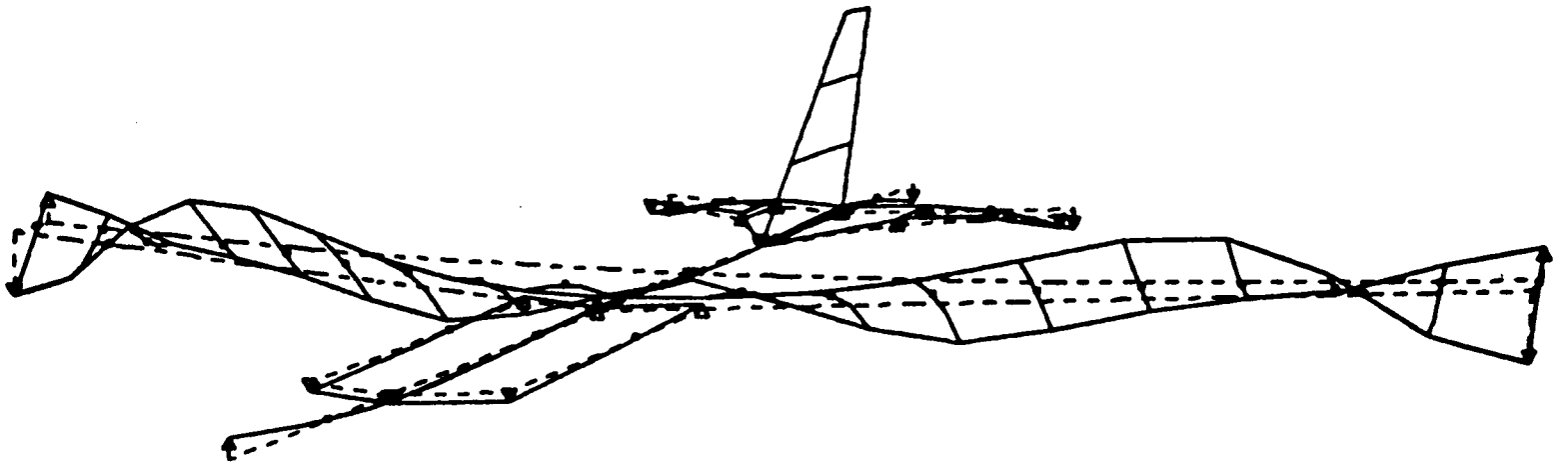

AREALS2.PL.XHT=313.75=XVT.197MODE=10. FREQ= 90.26HZ. GMASS= 0.

ACPO

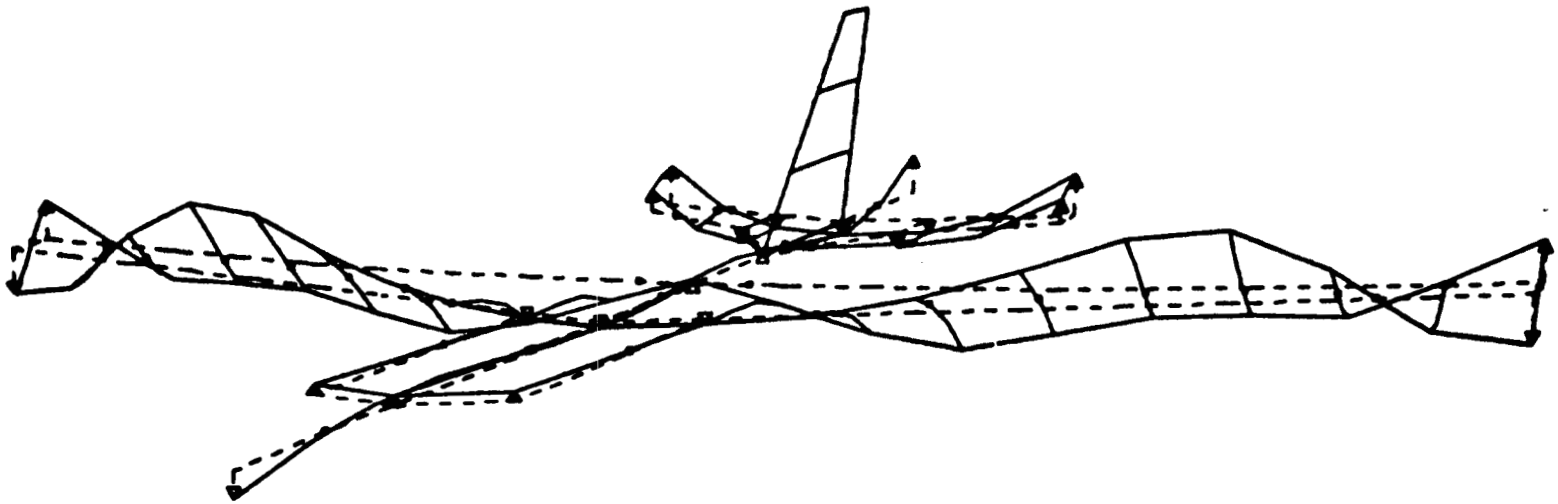

AREALS2.PL,XHT=313.75=XVT,197MODE=11. FREQ= 95.64HZ. GMASS= 0.

ACPO

Standard Bibliographic Page

1. Report No.	2. Government Accession No.	3. Recipient's Catalog No.
NASA CR-4071		

4. Title and Subtitle	5. Report Date
Eigenspace Techniques for Active Flutter Suppression	June 1987
	6. Performing Organization Code
7. Author(s)	8. Performing Organization Report No.
William L. Garrard, Bradley S. Liebst, and Jerome A. Farm	
9. Performing Organization Name and Address	10. Work Unit No.
University of Minnesota Department of Aerospace Engineering and Mechanics Minneapolis, MN 55455	11. Contract or Grant No. NAG1-217
12. Sponsoring Agency Name and Address	13. Type of Report and Period Covered Contractor Report 10/81 - 6/86
National Aeronautics and Space Administration Washington, D.C. 20546-0001	14. Sponsoring Agency Code 505-66-01-02

15. Supplementary Notes

Langley Technical Monitor: William M. Adams
Final Report

16. Abstract

This report discusses the use of eigenspace techniques for the design of an active flutter suppression system for a hypothetical research drone. One leading edge and two trailing edge aerodynamic control surfaces and four sensors (accelerometers) are available for each wing. Full state control laws are designed by selecting feedback gains which place closed loop eigenvalues and shape closed-loop eigenvectors so as to stabilize wing flutter and reduce gust loads at the wing root while yielding acceptable robustness and satisfying constraints on rms control surface activity. These controllers are realized by state estimators designed using an eigenvalue placement/eigenvector shaping technique which results in recovery of the full state loop transfer characteristics. The resulting feedback compensators are shown to perform almost as well as the full state designs. They also exhibit acceptable performance in situations in which the failure of an actuator is simulated.

17. Key Words (Suggested by Authors(s))	18. Distribution Statement
Flutter Suppression Feedback Control Eigenspace Aeroelastic Control	Unclassified - Unlimited Subject Category 08

19. Security Classif.(of this report)	20. Security Classif.(of this page)	21. No. of Pages	22. Price
Unclassified	Unclassified	64	A04

For sale by the National Technical Information Service, Springfield, Virginia 22161